PCA of Fe-oxides MLA data as an advanced tool in provenance discrimination and indicator mineral exploration: Case study from bedrock and till from the Kiggavik U deposits area (Nunavut, Canada)

Sheida Makvandi[a*], Georges Beaudoin[a], M. Beth McClenaghan[b], David Quirt[c], Patrick Ledru[c]

[a] Département de Géologie et de Génie Géologique, Université Laval, Québec (QC), Canada, G1V 0A6. (sh.makvandi@gmail.com; Georges.Beaudoin@ggl.ulaval.ca)

[b] Geological Survey of Canada, Ottawa (ON), Canada, K1A 0E8. (beth.mcclenaghan@canada.ca)

[c] Orano Canada Inc., 817 45th Street West, Saskatoon (SK), Canada, S7K3X5. (blquirt@gmail.com; patrick.ledru@orano.group)

*** Corresponding author:** Dr. Sheida Makvandi

Postal address: Département de géologie et de génie géologique, Université Laval, Pavillon Adrien-Pouliot, 1065 avenue de la Medecine, Québec (QC), Canada, G1V0A6

E-mail address: sh.makvandi@gmail.com

Keywords: Fe-oxide, Kiggavik, Till, MLA, PCA, Grain size, Mineral association

Abstract

Magnetite and hematite grains from the 0.25-0.5 mm and 0.5-2.0 mm ferromagnetic fractions of ten till samples collected up-ice, overlying and down-ice of the Kiggavik U deposits (Nunavut, Canada), as well as eight bedrock samples from Kiggavik igneous and metasedimentary basement and overlying sedimentary rocks were characterized for their grain size and mineral association using optical microscopy, scanning electron microscopy (SEM) and mineral liberation analysis (MLA). Principal component analysis (PCA) was used to evaluate the MLA data for Fe-oxide mineral association and grain size distribution. PCA shows that mineralogical and granulometric differences in Fe-oxides from Kiggavik igneous rocks distinguish them from that of Kiggavik metasedimentary and sedimentary rocks. In addition, The PCA results indicate that the composition and abundance of minerals associated/intergrown with Fe-oxides are not only different in various till samples, but also in different size fractions of the same sample. Higher proportions of hornblende, quartz, gahnite, grunerite, apatite, chromite and sulfides are intergrown with Fe-oxides in the 0.5-2.0 mm till fraction, as compared to the 0.25-0.5 mm fraction in which Fe-oxides are mostly associated with pyroxene, titanite, rutile, feldspars, calcite and zircon. The mineral associations and grain sizes of proximal bedrocks are reflected in smaller size fractions of Kiggavik till, whereas detrital grains in the 0.5-2.0 mm fraction of Kiggavik till may have originated from distal sources. PCA also shows that Fe-oxides from the Kiggavik bedrock and till can be discriminated from those of volcanogenic massive sulfide (VMS) deposits because of smaller grain sizes and higher abundances of sulfides, gahnite, axinite, corundum, hypersthene and pyroxene intergrown with VMS Fe-oxides. This study emphasizes the importance of selecting suitable representative grain size fractions of till, or other sediments, when using indicator minerals for exploration. The results of PCA of Fe-oxides MLA data are consistent with the results of using Fe-oxides geochemical data in provenance discrimination of Kiggavik till.

1. Introduction

In the past 30 years, breakthroughs have been achieved in the use of indicator minerals in the exploration for Au, Cu, Ni, PGE, Pb-Zn, and diamonds (e.g. Averill, 2001; McClenaghan and Kjarsgaard, 2007; Kaminsky and Belousova, 2009; McClenaghan et al., 2015; McClenaghan and Paulen, 2017). A great advantage of indicator mineral methods is the ability to trace the dispersion of eroded mineral deposits in surficial sediments. The presence of some minerals (e.g., omphacite, Cr-rich pyrope, and manganiferous ilmenite) in sediments indicates the potential to find specific deposits (e.g. fertile kimberlitic bodies). In the case of ubiquitous indicator heavy minerals such as Fe-oxides, their trace elements and isotope geochemistry can be used as a provenance discrimination and/or mineral exploration tool (Dupuis and Beaudoin, 2011; Boutroy et al., 2014; Dare et al., 2014; Nadoll et al., 2014; Makvandi et al., 2016a,c, 2017). The extent of elemental substitution and the type of substituting elements in Fe-oxides are strongly controlled by the environment in which they formed. Given that Fe-oxides are major to accessory minerals in many types of mineral deposits/geologic settings, their composition has widely been used to distinguish various mineral deposit types including Ni-Cu, Fe-Ti, volcanogenic massive sulfide (VMS), porphyry Cu, iron oxide copper gold (IOCG), iron oxide-apatite (IOA), banded iron formation (BIF), skarn, and unconformity-related U deposits (Dupuis and Beaudoin, 2011; Nadoll et al., 2014; Dare et al., 2014; Makvandi et al., 2016a,c, 2017). In contrast, the use of Fe-oxide mineral associations and grain size distribution in the identification of host mineral deposits is not well understood. Makvandi et al. (2015, 2016b) showed that the abundance of some minerals in association with magnetite helps to distinguish the composition of host rocks. They concluded that detrital Fe-oxides intergrown with gahnite, sillimanite and ilmenite were most likely derived from metamorphosed VMS deposits. Makvandi et al. (2015, 2016b) also reported that the shape and grain size of the Fe-oxides in till are fundamentally controlled by the grain's original shape and size ($\leq$ 0.25 mm to $\geq$ 1.0 mm) in host rocks, whereas the mode and duration of transport are secondary. Thus, they suggested that the study

of Fe-oxides shape and grain size can provide supplementary information to indicator mineral exploration programs.

This study aims to show the use of Fe-oxide mineral association and grain size distribution, obtained through mineral liberation analysis (MLA,) in provenance discrimination of till covering the Kiggavik U deposits area. To meet this objective, samples collected from various host rock compositions and from till collected at different distances from the Kiggavik deposits were studied using optical and electronic microscopy, as well as through mineral liberation analysis (MLA), an automated SEM-based mineralogy method. This study investigated the 0.25-0.5 and 0.5-2.0 mm fractions of Kiggavik till and will elaborate whether these size fractions of till are representative of Fe-oxides in Kiggavik host rocks, and thus, if they are suitable for further U exploration in the Kiggavik region.

1.1. Geologic setting

Regional and local geology

The Kiggavik camp is located in the northeast corner of the Thelon Basin (Nunavut, Canada; Figs. 1A-B), approximately 80 km west of Baker Lake (Hoffman, 1988). The Paleoproterozoic to Mesoproterozoic Thelon Basin is situated within the Rae Subprovince of the Western Churchill tectonic province of the Canadian Shield (Fig. 1B). The crystalline basement lithologies underlying the Kiggavik deposits comprise Archean granitoid gneiss, Neoarchean supracrustal rocks of the Woodburn Lake Group, metasedimentary and metavolcanic rocks of the Marjorie Hills Assemblage, the ~2.6 Ga Snow Island Suite (SIS), and the early Paleoproterozoic Ketyet River Group (Fig. 2A-B; Pehrsson et al., 2013; Tschirhart et al., 2013). These rocks have been variably metamorphosed from greenschist to amphibolite facies with common retrogression to greenschist facies (LeCheminant et al., 1979; Zaleski et al., 2000). Paleoproterozoic quartz arenites of the Amarook

Formation and the Thelon Formation of the Dubawndt Supergroup occurs several kilometers north of the Kiggavik deposits.

In the Kiggavik area, the quartzofeldspathic metagreywacke of the Pipedream Assemblage is structurally overlain by a sequence of Snow Island Suite quartz-feldspar porphyritic rhyolite (Pukiq Lake Formation), schist, and epiclastic metavolcanic phyllite, and Ketyet River Group metaquartzite (Fig. 2A-B; Scott et al. 2015; Sharpe et al. 2015; Johnstone et al., 2016, 2017). The uranium mineralization that characterizes the Kiggavik deposits is located at the gently-dipping interface between the overlying epiclastic-rhyolite-quartzite imbricate panel and the underlying Pipedream metagreywacke (Johnstone et al., 2017; Grare et al., 2018).

The western portion of the Kiggavik camp consists of the 1.83 Ga Hudson Igneous Suite (HIS) that comprises Hudson granite and Martell syenite formed as a result of mingling between lamprophyre and Hudson granite magmas (Tschirhart et al., 2013; Miller and Peterson, 2015). The Neoarchean to Paleoproterozoic basement rocks under the Thelon Basin were intruded by Paleo- to Mesoproterozoic, late-orogenic granite to ultrapotassic mafic to felsic dykes, laccoliths, and localized plugs of the Hudson and Kivalliq Igneous Suites (Fig.2A-B; Rainbird and Davis, 2007).

The Dubawnt Supergroup comprises three sedimentary sequences: the Baker Lake Group (1845–1785 Ma), Wharton Group (~1750 Ma), and Barrensland Group (<1720–1540 Ma; Rainbird et al. 2003). The crystalline basement rocks were deeply weathered and overlain by the aeolian to alluvial sandstone and conglomerate of the Amarook Formation, which forms the lower part of the Wharton Group. The Wharton Group is overlain by the Barrensland Group composed of fluvial, variably hematitic, quartz arenite, conglomerate and red mudstone of the Thelon Formation. The Thelon Formation is the dominant basin-filling unit of the Thelon Basin, and comprises three dominantly alluvial siliciclastic sequences (Hiatt et al. 2003; Tschirhart et al. 2014). The Thelon Formation was deposited on a paleo-regolith suggesting a significant depositional pause (Hiatt et al., 2010), and is locally capped by ultrapotassic basaltic flows of the Kuungmi Formation overlain by

siliceous stromatolitic dolostone of the Lookout Point Formation (Gall et al. 1992; Chamberlain et al., 2010). All lithologies in this region are cut by NW-trending 1.27 Ga Mackenzie dykes.

The Kiggavik area has been explored for uranium since the 1970s because the geology of the area is similar to that of the eastern part of the Athabasca Basin (Fuchs et al., 1985). The uranium deposits (Kiggavik, End, and Andrew Lake) and prospects (Bong, Granite, and Contact) in the Kiggavik region may be unconformity-related (Kiggavik Main and Central Zone deposits: Farkas, 1984; Shabaga et al., 2017; Bong deposit: Riegler et al., 2016a,b; Sharpe et al., 2015; Quirt, 2017; End deposit: Chi et al., 2017; Fayek et al., 2017), and are associated with multiple fault systems trending ENE–WSW (Thelon, Judge Sissons), NE–SW (Andrew Lake), and S-SE (Grare et al., 2018). These fault systems are sites of intense brittle deformation and alteration associated with hydrothermal activity. The Kiggavik deposit comprises three separate ore zones (Fig. 2A): (Main (MZ), Centre (CZ), and East zones (EZ), with resources estimated at approximately 50,000 t U at an average grade of 0.5 wt% (Jefferson et al. 2007). Fuchs and Hilger (1989) recognized that the mineralization at the Kiggavik deposits is intimately associated with intense clay mineral alteration halos that are hosted by mica-rich quartzofeldspathic metasediments (Pipedream Assemblage metagreywacke) and locally in Hudsonian granite. Uranium mineralization at the Kiggavik, Andrew Lake, and End deposits was originally described as uraninite altering to coffinite that indicates these deposits have experienced U remobilization (Fuchs et al. 1986; Sharpe et al. 2015; Shabaga et al. 2017). The U mineralization at the Bong deposit is also composed of uraninite, coffinite and paragenetically late uranyl minerals (e.g., uranophane; Riegler et al. 2014; Sharpe et al. 2015). Host-rock alteration related to the Kiggavik mineralization is generally characterized by strong bleaching of the host rock, chloritization, illitization, and hematitization extending over tens of meters (Fuchs and Hilger 1989; Riegler et al. 2014; Sharpe et al. 2015; Shabaga et al., 2017). The typical alteration mineral assemblage includes clay minerals (illite ± sudoite) ± hematite ± aluminum phosphates sulfates (APS), and quartz veining (Riegler et al., 2014; Sharpe et al., 2015).

Surficial geology

The Kiggavik region was covered by the Laurentide Ice Sheet from the beginning of the Wisconsinan through the Late Wisconsinan Maximum (18-13 Ka; Aylsworth and Shilts, 1989; Dyke et al., 2002; Dyke, 2004; McMartin and Henderson, 2004). The area was completely deglaciated between 7.2 and 6.0 Ka. Blocking of the Thelon River drainage by the retreating ice mass resulted in deposition of lake sediments in the Thelon River valley and Princess Mary Lake basin, approximately 60 km southeast of the Kiggavik deposits (McMartin and Dredge, 2005). No evidence of glaciofluvial sediments is recorded in the Schultz Lake area. In absence of eskers and ribbed moraines, a ubiquitous cover of till characterizes the surficial geology of the Kiggavik camp (Aylsworth and Shilts, 1989; McMartin et al., 2006; Robinson et al., 2014).

In the Kiggavik deposit area, bedrock highs are covered by thin layers of till, whereas lower lying areas, and less-resistant metasedimentary rocks are covered by hummocky till (Robinson et al., 2016). There is only 5% bedrock exposure, mainly in gentle hills that consist of Ketyet River Group quartzite, Neoarchean basement granitic gneiss, or Hudson granitic rocks (Robinson, et al., 2016). The Proterozoic quartzite exposures, situated north of the Kiggavik deposits, preserve faceted and striated surfaces that record multiple ice-flow trajectories (Robinson et al., 2016). Surficial mapping indicates that the Schultz Lake area has been affected by multiple phases of ice flows from which the Kiggavik area was dominantly affected by northwest and westnorthwest ice flows (Aylsworth and Shilts, 1989; Aylsworth et al., 1990; McMartin et al., 2006; Fig. 2C).

1.2. Fe-oxides in Kiggavik bedrock and till

Kiggavik bedrock

Makvandi et al. (2017) studied petrographic characteristics and trace element compositions of magnetite and hematite grains in unmineralized bedrock and till samples collected in the vicinity of the Kiggavik MZ deposit. The composition of these minerals from local bedrock lithologies was used to construct discriminant models that serve to classify the sources of Fe-oxides grains in Kiggavik till. Petrography and geochemical data suggest a magmatic origin for magnetite, the predominant Fe-oxide phase (Figs. 3A-C), in Kiggavik igneous basement rocks. Magnetite grains from the late-orogenic leucogranite, granite and Martell syenite samples of the Hudson and Kivalliq (Nueltin) Suites are hosted by the magmatic assemblage of feldspar, biotite, muscovite and hornblende (Fig. 3B), and are partly replaced by ilmenite. Cobalt, V, Cr, Pb and Ni are discriminant elements for the magmatic magnetite (Makvandi et al., 2017). In the Kiggavik igneous basement, hematite formed by replacing magnetite. Figure 3C shows a hematite pseudomorph after magnetite from the Hudson and Kivalliq Suites granite. Higher concentrations of Mg, Al, Ti, and Zr in the hematite relative to the parent magnetite suggests that hematite crystallized from high-temperature hydrothermal fluids. Zircon (Fig. 3C) and apatite are abundant accessory minerals in association with Fe-oxides in the Kiggavik igneous basement rocks.

In contrast to Kiggavik igneous basement, hematite is the dominant Fe-oxide, assumed to be mainly a result of in situ replacement of magnetite and ilmenite (Figs. 3D, E). Specular hematite occurs in the Lower Ketyet River Group quartzite (Fig. 3D) filling vugs after dissolution of the host rock, suggesting that this hematite is hydrothermal, whereas, the SIS rocks contain detrital hematite grains (Fig. 3E). The Thelon Formation quartz arenite also contains detrital hematite grains (Fig. 3F) that are associated with different phases of quartz mineralization (host rock silicification). Makvandi et al. (2017) suggested that part of detrital hematite grains from the quartz arenite originate from the Kiggavik igneous basement as their trace element compositions resemble that of Fe-oxides from the

Hudson and Kivalliq (Nueltin) Suites leucogranite and granite.

Kiggavik till

Petrography and geochemical data suggest that Kiggavik till contains Fe-oxides from various host bedrock lithologies. Although magnetite is abundant in Kiggavik till, hematite is the dominant Fe-oxide. Magnetite is commonly granular and/or it occurs as altered material in different mineral assemblages, such as intergrowths with quartz and hematite (Fig. 4A). The assemblage of quartz, platy hematite, and almandine garnet replacing euhedral magnetite (Fig. 4A) suggests that the host rock underwent metamorphism. Some magnetite grains in Kiggavik till that might originate from igneous rocks are intergrown with ilmenite and mafic minerals, such as clinopyroxene and orthopyroxene (Fig. 4B), or occur in association with quartz and apatite (Fig. 4C). Figure 4D illustrates a polymineralic aggregate from Kiggavik till composed of subhedral magnetite grains as well as magnetite-rutile symplectite and Mn-rich ilmenite islands filling dissolution pits. The Fe-Ti oxides intergrowths are partly replaced by titanite (Fig. 4D). In Kiggavik till, hematite occurs as veinlets or disseminated grains in quartz aggregates as well as specular or botryoidal hematite in polymineralic particles. Occurrence of specular hematite in association with quartz resembles the mineralogy and textures of hematite in Ketyet River Group quartzite (Robinson et al., 2016). Hematite pseudomorphs after magnetite that are associated with clay minerals (Fig. 4E) suggest Kiggavik metasedimentary basement rocks as the potential source of the till grains. In contrast, sulfide inclusions in hematite pseudomorphs (Fig. 4F) resemble the mineralogy of the HIS mafic syenite (Makvandi et al., 2017). Although many studies showed the close association between Fe-oxides and U-bearing minerals in the Kiggavik deposits and prospects (e.g., Chi et al., 2017; Shabaga et al., 2017; Grare et al., 2018), petrography indicates that U-bearing minerals are absent in the 0.25-2.0 mm F-HMC of Kiggavik till. Makvandi et al. (2018) showed that U-bearing minerals (mostly uraninite and coffinite) are not intergrown with hematite and/or goethite in mineralized bedrock

samples from the Kiggavik-Andrew Lake structural trend deposits.

2. Methods

2.1. Sample selection and preparation

The Geological Survey of Canada (GSC) collected a total of forty-two bedrock and seventy-one bulk till samples in the Kiggavik area during the summer of 2010; a portion of the bedrock and till samples was sent to the Overburden Drilling Management Limited (ODM; Ottawa, Canada) to produce heavy mineral concentrates (HMC; Robinson et al., 2016). Bedrock samples were disaggregated using electric pulse disaggregation (EPD). The morphology of the liberated minerals is expected to reflect their original shape and grain size in the bedrock (Rudashevski et al., 2002; Cabri et al., 2008). The preparation of ferromagnetic heavy mineral fractions (F-HMC) from disaggregated bedrock and till samples is described in McClenaghan et al. (2012). The F-HMC of till samples were sieved to produced 0.25-0.5 mm and 0.5-2.0 mm fractions, and the < 0.25 mm fraction was archived. From the GSC Kiggavik samples, the 0.25-0.5 mm and 0.5-2.0 mm fractions of ten F-HMC till samples, the 0.25-2.0 mm fractions of four F-HMC bedrock samples as well as offcuts of four other bedrock samples were sent to the Université Laval to study geochemical and mineralogical characteristics of Fe-oxides. Descriptions of the studied bedrock and till samples are in Table 1. The eight Kiggavik bedrock samples are from Snow Island Suite (SIS) epiclastic rocks (n=1), Lower Ketyet River Group quartzite (n=1), Hudson and Kivalliq Suites leucogranite (n=1) and granite (n=1), Martell syenite (n=1), Hudson Igneous Suite (HIS) mafic syenite (n=1), and Thelon Formation quartz arenite (n=2). The location of studied bedrock and till samples is shown in Figures 2A and C. The Kiggavik till samples are from locations up-ice, overlying, and down-ice (NW and WNW directions) of the Kiggavik MZ. Twenty-five polished grain mounts and four polished thin sections

were made of the given bedrock and till samples.

2.2. Analytical methods

The Kiggavik bedrock and till samples were investigated using MLA that was carried out on a FEI Quanta 400 W instrument at Memorial University (Newfoundland, Canada) with a Bruker EDX and the Esprit software. Instrument parameters were 25 kV, spot size 7.94 μm, 1.5 mm HFW (horizontal field width), and working distance of 12 mm. The beam current was 13 nA, 16 microseconds BSE (back-scattered electron) dwell time, 500 dpi frame resolution, and 20 millisecond spectral dwell time. Prior to MLA, magnetite and hematite grains from the Kiggavik bedrock and till samples were studied and photographed using optical microscopy and were analyzed by scanning electron microscopy (SEM) to determine their textural relationships with mineral associations. The petrographic and SEM results were used to develop the library of reference spectra before MLA and also to validate MLA results.

2.3. Multivariate statistical approaches to MLA data analysis

The MLA grain size distribution and mineral association data for the Fe-oxides from the Kiggavik bedrock and till samples were analyzed by principal component analysis (PCA). Traditionally, MLA data are analyzed by conventional data presentation methods, such as box and whisker diagrams, histograms, pie charts and/or cumulative passing plots (Sylvester, 2012; Makvandi et al., 2015). In contrast, PCA is a mathematical procedure that is used to reduce a large set of possibly correlated variables to a smaller number of uncorrelated variables called principal components that still contains important information from the original dataset (Wishart, 2013). A principal component (PC) factor is a linear combination of the original variables that is weighted by their contribution to explaining the variance in a particular orthogonal dimension (Geladi et al., 1989; Geladi and Grahn,

1996). The first factor (PC1) explains the greatest possible portion of the variance within the dataset, whereas the second factor (PC2) captures the second largest variance orthogonal to the first, and so on. PCA factor loadings are the correlation coefficients between the original variables and the PC and represent the percent of variance in a given variable that is explained by the PC. Factor loadings provide information on the impact of a particular variable (e.g., the abundance of a mineral of interest) on a given factor (Geladi et al., 1989; Geladi and Grahn, 1996). The sign of loadings (positive or negative) is used to interpret the correlation between variables (e.g., Fe-oxide grain size and/or the abundance of mineral associations). Loadings are depicted on factor plots (PC1 versus PC2, PC1 versus PC3, etc.). PCA scores are composite values for each observation on each factor extracted in the factor analysis. Factor weights are used in conjunction with the original variable values to calculate each observation's score which are standardized to reflect a z-score (Geladi et al., 1989; Geladi and Grahn, 1996). Factor scores place each variable in a plane of multivariate variability and are depicted on score plots (t_1 versus t_2, t_1 versus t_3, etc.). In fact, the score plot is a scatter plot, and involves the projection of the data onto the PCs in two dimensions. The x axis contains a user-selected PC (e.g., PC1), while the y axis contains another user-selected PC (e.g., PC2). In this study, PCA was applied to reduce the dimensionality of the large MLA datasets, to reveal hidden correlations among variables, and to identify variables potentially useful in classifying sources of Fe-oxides in the till samples.

3. Results

MLA produces datasets that include modal mineralogy, particle (polymineralic aggregate) size distribution and particle properties (containing values of particles angularity, area, perimeter, aspect ratio and form factor) that can be viewed using the DataView software (Fandrich et al., 2007).

In addition, to characterize a mineral (assemblage) of interest, respective data subsets of grain size and/or grain properties and mineral associations can be generated. Figure 5 is a MLA false-color image of Fe-oxide grains from Kiggavik till illustrating that Fe-oxides in F-HMC of Kiggavik till may occur as liberated grains (Fig. 5A) or they may be intergrown with other minerals (Figs. 5B-C). Figure 5B shows an Fe-oxide aggregate containing micro-inclusions of quartz, chlorite, spinel, amphibole, gahnite and zeolite, whereas in Figure 5C, Fe-oxides are fine-grained (< 0.02 mm) components of a polymineralic aggregate formed by quartz, almandine garnet and clay intergrowths. The Fe-oxides have been replaced by clay minerals along their edges and also contain apatite inclusions (Fig. 5C).

MLA computes values for the maximum length of mineral grains and the grain size distribution for classes based on physical sieve sizes (Sylvester, 2012). Grain size data for the Kiggavik bedrock and till samples are cumulative percentages of values obtained from Fe-oxide grains in each sample passing different sieve sizes. The grain size data are subject to the constant-sum constraint (Aitchison, 1986), so the data were centered log-ratio (clr) transformed prior to PCA to overcome the closure effect (Aitchison, 1986; Flood et al., 2015).

In this study, the data subsets of Fe-oxide grain size and mineral associations from different bedrock and till samples were integrated and then investigated by PCA to demonstrate the use of indicator minerals MLA data analysis in provenance discrimination and in mineral exploration, (Figs. 6-8). Grain size was considered to be an important variable because the MLA results showed that the size of Fe-oxides in each size fraction (0.25-0.5 mm and 0.5-2.0 mm) of the till samples also varies over a wide range depending on the form of minerals occurrence (e.g., liberated grains or inclusions in other minerals aggregates). However, the MLA results revealed that liberated Fe-oxide grains are mostly present in the smaller size fraction of tills, whereas in the larger size fraction, Fe-oxides occur in polymineralic aggregates.

3.1. Mineral associations and grain size of Fe-oxides from Kiggavik bedrock

An integrated dataset of mineral associations and grain size of Fe-oxides from the bedrock samples were investigated by PCA. Only the results of analysis of the first and second PCs are depicted in Figure 6 because they explain forty-two and fifteen percent of the total variance within the MLA dataset, respectively. Smaller portions of the 45% remaining variance were captured by the succeeding factors (e.g., 8 % by PC3). In Figure 6A, factor loadings in the PC1-PC2 space illustrate the correlations between variables (Fe-oxide grain size, and the abundance of mineral associations). Grain sizes and/or minerals plotted in the vicinity of each other in this factor space show strong positive correlations, and they are negatively correlated to grain sizes and/or minerals plotted in the opposite quadrant. In Figure 6A, grain sizes of 425 to ≥ 1000 μm plot with orthopyroxene, chromite, Cr-rich magnetite and spinel in the low PC1 and PC2 values region, that means coarse Fe-oxides from the Kiggavik bedrock samples are mostly interlocked with the given minerals. In contrast, biotite, muscovite, chlorite and zeolite that plot in high PC1 values region are dominant in association with fine-grained Fe-oxides (9.6 to 250 μm).

Figure 6B illustrates the distribution of the Kiggavik bedrock samples in t_1-t_2 scores space. In the PCA scores plot, samples that plot in the vicinity of each other share similar grain size distributions and mineralogy. As a result, PC1 separates Fe-oxides from the igneous basement samples (granite, leucogranite, mafic syenite and Martell syenite) and those from the metasedimentary basement samples (quartzite and epiclastic rocks) and Thelon Formation quartz arenites because of distinct differences in mineralogy and grain size distribution (Figs. 6A-B). The igneous basement rocks are mainly characterized by small grain sizes (≤ 5.7 to 350 μm) and are associated with minerals such as Ti-bearing minerals (e.g., ilmenite, rutile, titanite), feldspars (anorthite, albite, orthoclase), garnet, apatite and zircon (Figs. 6A-B). Figure 6A indicates that clay minerals, gahnite, clinopyroxene and staurolite have no impact on the sample distribution in Figure

6B.

3.2. Mineral associations and grain size of Fe-oxides from Kiggavik till

In Figure 7A-B, PCA shows the relationships between grain size distribution and abundance of mineral associations of Fe-oxides from the till samples. In this analysis, fifty-five percent of the total variance within the MLA dataset analyzed was captured by the first and second principal components. The PC1-PC2 factor loadings plot (Fig. 7A) demonstrates the close spatial association between quartz and 300-500 μm grain size on the upper left quadrant that means quartz is the dominant mineral association of 300-500 μm Fe-oxide grains. In contrast, Figure 7A indicates that ilmenite and titanomagnetite are mostly intergrown with 600 μm grains. The PCA scores (Fig. 7B) also show that the abundance of mineral associations and variable grain sizes differentiate between Fe-oxides from different fractions of the Kiggavik till samples. As a result, the smaller size fraction (0.25-0.5 mm) of Kiggavik till, except for sample 10-PTA-115 (Till 115), are clustered in the low t_1 region mostly because of their smaller grain size, and higher abundance of Ti-bearing minerals, clays, calcite, zircon and feldspars. In contrast, higher abundance of hornblende, biotite, apatite, gahnite, chromite and sulfides in association with coarse Fe-oxide grains (710- ≥ 1000 μm) discriminates the 0.5-2.0 mm fraction of Kiggavik till.

PCA separates the 0.25-0.5 mm fraction of Till 115 from the other till samples in the high t_1 value region in Figure 7B. Figure 7A indicates that the separation of small fraction size of Till 115 is due to the very fine-grained nature (≤ 5.7 to 250 μm) of Fe-oxides and higher abundance of garnet, chlorite, orthopyroxene, staurolite and muscovite associated with Fe-oxides in this samples. The 0.25-0.5 mm fraction of sample 10-PTA-128 (Till 128) is isolated in the low t_1, t_2 region of Figure 7B because of the higher abundance of titanite, rutile, clays, zircon, feldspars and spinel intergrown with Fe-oxides, whereas the 0.5-2.0 mm fraction of sample 10-PTA-112 (Till 112) is mainly

separated by PC2 in the high t_2 region due to the distinct grain size distribution of Fe-oxides (300, 710 and 850 μm) and the higher abundance of hornblende, grunerite, gahnite, sulfides and chromite.

A data subset of mineral associations and grain size of Fe-oxides from the bedrock and till samples was investigated by PCA to determine whether the Kiggavik till shares similar mineralogy and grain size distribution as the local bedrock. In Figure 8, the first and second PC factors represent fifty percent of the total variance in the MLA dataset. As shown in Figure 8A, the larger grain sizes (710 to ≥ 1000 μm) plot in the vicinity of hornblende, apatite, epidote, Cr-rich magnetite, chromite and gahnite in the high PC2 values region (Fig. 8A), whereas the 9.6 to 250 μm grain sizes are isolated in the higher PC1 values region and show a close association with chlorite, biotite and muscovite. The correlation among Fe-oxides grain sizes and the abundance different minerals in association with them in Figure 8A resulted in discrimination the 0.25-0.5 mm and 0.5-2.0 mm fractions of Kiggavik till in Figure 8B as the coarser size fraction of the till samples mostly plot in the high t_1 region, whereas the smaller size fraction of the till samples are mostly clustered in the low t_1 region. In addition, quartz arenite (R020), quartzite and mafic syenite plot in the vicinity of the smaller size fraction of Kiggavik tills (Fig. 8B). Higher abundance of titanite, sulfides, zircon, rutile and calcite in association with 300 μm Fe-oxide grains (in the low PC1, PC2 region of Fig. 8A) differentiate granite, leucogranite, quartz arenite (R018) and Martell syenite (in the low t_1, t_2 region of Fig. 8B) from the Kiggavik till samples. Whereas PC1 separates the epiclastic bedrock and the small size fraction of Till 115 (in the high t_1 region) from the other till and bedrock samples (Fig, 8B), different PC2 values differentiate them in the t_1-t_2 space (Fig. 8B).

4. Discussion

The petrographic and MLA results show that Fe-oxides from the Kiggavik bedrock and till

samples are characterized by variable grain size distributions and mineral associations (Figs. 3-5). However, some Fe-oxides from the till samples show mineralogical and granulometric characteristics similar to those from studied bedrock suggesting that they may originate from proximal sources. For example, the replacement of magnetite by hematite and/or quartz (Figs. 4A-B) is similar to the alteration history of Kiggavik bedrock (Riegler et al., 2014; Robinson et al., 2014; Makvandi et al., 2017). Veins or disseminated hematite associated with widespread quartz ± clay minerals are also characteristic signatures of Kiggavik metasedimentary basement rocks (Robinson et al., 2016). The replacement of magnetite by titanite (Fig. 4D) may indicate the igneous basement as the bedrock source of the grain (Robinson et al., 2014; Makvandi et al., 2017).

Despite the focus being on the 0.25-0.5 mm and 0.5-2.0 mm F-HMC of the Kiggavik tills, the MLA revealed that more than 1.5 % of Fe-oxide grains in the till are ≤ 5.7 μm in size and form parts of larger multi-mineralic grains. These Fe-oxides occur either as liberated grains (5A) or as inclusions in other minerals (Fig. 5C), thus, their grain size in each fraction size is also variable, as grains < 0.25 mm and < 0.5 mm are observed in the 0.25-0.5 mm and 0.5-2.0 mm fractions of Kiggavik tills, respectively.

4.1. Bedrock sample discrimination using PCA of Fe-oxides MLA data

Figures 6A-B show that PCA can differentiate between Fe-oxides from different Kiggavik bedrock lithologies due to their different mineral association and grain size. PCA indicates that higher abundances of orthoclase, ilmenite, titanite, apatite, zircon, grunerite, albite, chlorite, calcite, and the 300 μm grain size are discriminant variables for Fe-oxides from the Kiggavik igneous basement, whereas higher abundance of grunerite, quartz, spinel, titanomagnetite and ilmenite, and the 425, 500, 600, and 710 μm grain sizes separate quartz arenite from the igneous and metasedimentary basement rocks (Figs. 6A-B). Makvandi et al. (2017) showed that in Kiggavik granite, leucogranite,

and Martell syenite, ilmenite partly formed at the expense of magnetite grains and the disequilibrium textural relationship between the Fe-Ti oxides in given rocks is consistent with the complex history of formation and emplacement of the Nueltin granites and associated Kivalliq Suite mafic rocks (Scott et al., 2015; Peterson et al., 2015). Fe-oxides from the Kiggavik igneous rocks contain zircon inclusions that were most likely inherited from Archean to Early Paleoproterozoic basement rocks. Although Fe-oxides from Kiggavik igneous basement are separated by PC2 from that of sedimentary and metasedimentary rocks, they also show distinct mineralogical and granulometric signatures. For example, leucogranite plots in the high t_2 scores region, making an impact on the classification model mainly due to the higher proportion of 355 μm Fe-oxide grains, and the greater abundance of ilmenite, rutile, titanite, apatite, zircon, grunerite, anorthite and calcite intergrown with Fe-oxides (Figs. 6A-B). Robinson et al. (2016) showed the close association of magnetite and hematite grains with plagioclase, amphiboles and Ti-bearing minerals in the leucogranite. They also indicated that fine-grain pyrite (< 0.1 mm) occurs in trace amounts (< 1%) in leucogranite, consistent with the results in Figure 6A that suggest sulfides are not important in discrimination of leucogranite Fe-oxides from that of the other bedrock samples. In contrast, PCA shows that Fe-oxides from the mafic syenite sample are mainly discriminated from other rock types because of intergrowths with sulfides and hornblende (Fig. 3B), consistent with the earlier suggestion that magmatic magnetite from the HIS mafic syenite was formed partly by replacement of early crystallized sulfides (e.g., pyrite and chalcopyrite) and silicates (Makvandi et al., 2017).

4.2. Provenance discrimination of Fe-oxides from Kiggavik till using PCA of MLA data

PCA of integrated mineral association and grain size of Fe-oxides discriminates different samples and size fractions of till samples (Figs. 7A-B). This suggests that Fe-oxides from the finer

size fraction of the Kiggavik till samples represent different host rock lithologies than Fe-oxides from the coarser size fraction. In the PCA t_1-t_2 scores space (Fig. 7B), Till 115 (0.25-0.5 mm), collected 50 m down-ice (WNW) of the Kiggavik MZ (Fig. 2), is well discriminated from the other till samples because of the fine-grained nature of its Fe-oxides as well as high abundance of garnet (mostly almandine), staurolite, chlorite, orthopyroxene, and muscovite intergrown with Fe-oxides. This mineral assemblage is typical for metamorphic rocks such as metamorphosed schists, greywacke and/or pelitic rocks (Bucher and Frey, 2002; Suk, 2013), and consistent with the mineral composition of metasedimentary rocks of the Woodburn Lake Group hosting the Kiggavik deposits (Jefferson et al., 2007; Scott et al. 2015; Sharpe et al. 2015). PCA scores also plot Till 128 (0.25-0.5 mm), collected 500 m down-ice (NW) of the Kiggavik MZ (Fig. 2), in the low t_1, low t_2 region because of the higher abundance of rutile, spinel, titanite, clay minerals and zircon intergrown/associated with Fe-oxides (Figs. 7A-B). The rutile-spinel-titanite-clay-zircon assemblage observed in Till 128 (0.25-0.5 mm) is representative of the Kiggavik deposits (Makvandi et al., 2018) as well as sandstone/basement hosted U deposits in the Athabasca Basin (Campbell, 2009). In contrast, the 0.5-2.0 mm fraction of till sample 10-PTA-112, collected 500 m down-ice (WNW) of the Kiggavik MZ (Fig. 2), contains greater abundances of coarse Fe-oxide grains intergrown with gahnite, sulfides, chromite, grunerite and hornblende (Figs. 7A-B). This mineral assemblage suggests that these till Fe-oxide grains were likely derived from distal bedrock source(s) potentially associated with metamorphosed VMS mineralization. Gahnite occurs in and around moderate to high grade metamorphosed massive sulfides and VMS deposits, and it is used as an indicator mineral in till for these deposit types (O'Brien et al., 2015; McClenaghan et al., 2015). Makvandi et al. (2017) also suggested VMS-related banded iron formations (BIF) as the potential source for part of Fe-oxide grains in Kiggavik till because trace element compositions of these Fe-oxides resemble that of the Izok Lake BIF. In addition, the mineral exploration program undertaken by Aura Silver Resources Inc. in 2009 in the area of Greyhound Lake detected the signature of VMS mineralization about 60 km north of Baker Lake (Boaz, 2009).

PCA results of the integrated MLA data of Fe-oxides from the Kiggavik bedrock and till samples, show that the bedrock samples plot in the same factor space as the smaller size fraction of Kiggavik tills (Figs. 8A-B). This result is consistent with the results shown in Figures 7A-B that detected the signature of the Kiggavik deposits and local metamorphic bedrock in the smaller size fraction of Till 128 and Till 115, respectively, but identified the signature of distal sources in the larger fraction of Till 112. Given the proximity of the HIS mafic syenite, quartzite and quartz arenite (R020) to the 0.25-0.5 mm fraction of Kiggavik tills in the PCA t_1-t_2 space (Fig. 8B) that is practically resulted from similar mineral association and grain size of Fe-oxides, these bedrock lithologies might be the source of higher proportion of Fe-oxide grains in the smaller size fraction of the tills. The PCA results in Figures 8A-B also suggest that the contribution of the other studied bedrock samples such as granite, leucogranite, Martell syenite and quartz arenite (R018) in feeding Fe-oxides to the local till might be much less than the previous bedrock samples. However, trace element geochemistry of Fe-oxides indicated that part of detrital Fe-oxides in Thelon Formation quartz arenite are the product of weathering, erosion and local transportation of Kiggavik igneous basement (Makvandi et al., 2017). The isolation of Till 115 (0.25-0.5 mm) in the high t_2 scores region of Figure 8B indicates that the source of Fe-oxide grains in this sample not only differs from that of Fe-oxides from the other till samples, but that also none of studied bedrock lithologies is the potential source of the grains.

Unlike quartzite, mafic syenite and quartz arenite (R020), PCA plots the SIS epiclastic rocks in the high t_1, low t_2 scores region in Figure 8B mainly because of higher proportions of fine-grained ($\leq$ 250 µm) Fe-oxides in this sample (Fig. 8A). The large difference between the grain size distribution of Fe-oxides from the SIS epiclastic rocks and that of till Fe-oxides suggests that the signature of this lithology is misrepresented in both fractions of Kiggavik till analyzed in this study.

To evaluate the utility of PCA of MLA data in provenance discrimination of the Kiggavik till Fe-oxides, the results were compared to the results of PCA of trace element compositions of Fe-oxides from the same bedrock and till samples (Makvandi et al., 2017; Figs. 9A-B). As shown in

Figure 9B, the fields occupied by all Kiggavik bedrock samples other than the fine-grained (≤ 250 µm) hematite from the epiclastic rocks are occupied by Kiggavik till Fe-oxides that means the geochemical signatures of Fe-oxides from these bedrocks can be detected in the till. Makvandi et al. (2017) measured 370 to 600 ppm U in hematite from the epiclastic rocks. This emphasizes on the importance of missing the signature of this lithologie in till. Robinson et al. (2016) showed that the <0.063 mm fractions of Till 115 and Till 128 (representing till matrix) contain anomalous concentrations of U, Ti, Ag, Co, Mo, Ni, and Cu. This geochemical signature of Kiggavik mineralization in the till matrix, and small sizes of U-rich hematite from the SIS epiclastic rocks (≤ 250 µm) suggest that Fe-oxides associated with U mineralization might occur in the < 0.063 mm fraction of the Kiggavik tills. Figures 9A-B shows that some till Fe-oxides that could originate from distal bedrock sources, plotting in the high t_1, low t_2 region of Figure 9B, contain higher Mg, Si, Ca, Al, Ti, Ge and Ga. Makvandi et al. (2016c) also identified Si, Ca, Al, Ga, Mg, and Ti as discriminant elements for Fe-oxides from VMS mineralization and respective alteration zones.

4.3. Application of Fe-oxides MLA data to mineral exploration

PCA was initiated to compare mineral association and grain size MLA data of Fe-oxides from the bedrock and till samples with Fe-oxides MLA data from bedrock and till collected from the vicinity of the Halfmile Lake (New Brunswick, Canada; Makvandi et al., 2012) and Izok Lake VMS deposits (Makvandi et al., 2015; Figs. 10A-B). PCA shows that the Izok Lake and Halfmile Lake bedrock and till samples form a distinct cluster in the low t_1, t_2 scores region because of the higher proportions of coarse Fe-oxide grains (425- ≥ 1000 µm), and greater abundance of muscovite, sulfides, orthopyroxene, gahnite, axinite and corundum in association with the Fe-oxides (Figs. 10A-B). Unlike the tight field formed by the VMS samples, Fe-oxides from the Kiggavik bedrock and till samples plot over a larger area in the t_1-t_2 scores space because of the diversity in mineralogy and grain size of the Fe-oxides (Figs. 10A-B). The classification model formed by PCA of Fe-oxide MLA

data from the Kiggavik, Izok Lake, and Halfmile Lake areas is significantly affected by very small grain sizes of Fe-oxides from the SIS epiclastic rocks relative to that of the other samples (Figs. 10A-B). The results in Figures 10A-B indicate that different geologic settings can be differentiated based on specific mineral association and grain size of Fe-oxides. In addition, these results demonstrate that the success of indicator mineral exploration programs very much depends on selecting suitable size fractions of till or other sediments to sample and study.

5. Conclusions

This study demonstrates the potential of using Fe-oxides mineral association and grain size data in provenance discrimination of unconsolidated sediments. The analysis of Fe-oxides MLA data indicates that mineralogical signatures of Kiggavik bedrock lithologies are reflected mostly in the 0.25-0.5 mm fraction of Kiggavik till. In till samples that reflect the metasedimentary basement rocks, 0.25-0.5 mm Fe-oxide grains mainly occur integrown with almandine, staurolite, chlorite and orthopyroxene. The results suggest that Fe oxides in the larger size fraction of till might originate from distal bedrock sources, potentially associated with VMS mineralization. PCA of Fe-oxides bedrock and till MLA data differentiates between the Kiggavik samples from that of the Halfmile Lake and Izok Lake VMS deposits. This study shows that the MLA results agree with the till Fe-oxides geochemical results. The latter suggests that a combination of MLA and geochemical data may improve indicator mineral exploration programs using Fe-oxides. PCA of MLA data also demonstrated that the signature of certain bedrocks of interest, such as Snow Island Suite epiclastic rocks, are misrepresented in the 0.25 to 2.0 mm fraction of Kiggavik till due to small grain sizes of Fe-oxides in these rocks. Thus, characterizing the grain size distribution of indicator minerals in deposits and/or lithologies is critical for selecting representative particle-size fractions of till or stream sediments for application of indicator mineral analysis in exploration.

Acknowledgements

This research was funded by the NSERC-Agnico Eagle Industrial Research Chair in Mineral Exploration. We acknowledge the earlier field work and research by S. Robinson (University of Queen's) on the Kiggavik area rocks and till samples and his sharing of data for the current study. We would like to thank all who collaborated on this project including M. Ghasemzadeh-Barvarz (Ingredion Incorporated), M. Choquette (ULaval), A. Ferland (ULaval), E. Rousseau (ULaval), D. Grant (MUN) and D.J. Goudie (MUN). John Robbins and Craig Cutts (Orano Canada) are also thanked for their insightful reviews of this manuscript.

References

1. Aitchison J., 1986. The Statistical Analysis of Compositional Data. Chapman and Hall, London, 416 pages.
2. Averill S.A., 2001. The application of heavy indicator minerals in mineral exploration. In Drift Exploration in Glaciated Terrain, M.B. McClenaghan, P.T. Bobrowsky, G.E.M. Hall, and S. Cooks (eds.). Geological Society of London Special Publication 185, 69-82.
3. Aylsworth J.M., and Shilts W.W., 1989. Glacial features around the Keewatin Ice Divide: Districts of Mackenzie and Keewatin. Geological Survey of Canada, Paper 88-24, 21 pages.
4. Aylsworth J.M., 1990. Surficial Geology, Aberdeen Lake, District of Keewatin, Northwest Territories, Geological Survey of Canada, Preliminary Map, Map number 44-1989.
5. Boaz R., 2009. In: Franklin, J.M. (Ed.), Update on Gold and Base Metal Targets at Greyhound Lake Property, Nunavut: Assays Return: 9.2% Copper, 18.5% Zinc, (2
6. pages).
7. Boutroy E., Dare S.A.S., Beaudoin G., Barnes S.J., Lightfoot P.C., 2014. Minor and trace element composition of magnetite from Ni-Cu-PGE deposits worldwide and its application to mineral exploration. Journal of Geochemical Exploration, 145, 64-81.
8. Bucher K., and Frey M., 2002. Petrogenesis of metamorphic rocks. Springer-Verlag Berlin Heidelberg, 341 pages, https://doi.org/10.1007/978-3-662-04914-3.
9. Cabri L.J., Rudashevsky N.S., Rudashevsky V.N., Oberthur T., 2008. Electric-pulse disaggregation (EPD), Hydroseparation (HS) and their use in combination for mineral processing 232 and advanced characterization of ores. Proceedings of the 40th Annual Canadian Mineral Processors Conference, Ottawa 2008, 221-235.
10. Chamberlain K.R., Schmitt A.K., Swapp S.M., Harrison T.M., Swoboda-Colberg N., Bleeker W., et al. 2010. In situ U-Pb micro-baddeleyite dating of mafic rocks: method with examples. Precambrian Research, 183, 379-387.
11. Campbell J.E., 2009. Drift prospecting for uranium in the Athabasca Basin, Saskatchewan, In: Application of till and stream sediment heavy mineral and geochemical methods to mineral exploration in Western and Northern Canada, (ed.) R.C. Paulen and I. McMartin; Geological Association of Canada, short course notes 18, 207-214.
12. Chi G., Haid T., Quirt D., Fayek M., Blamey N., Chu H., 2017. Petrography, fluid inclusion analysis, and geochronology of the End uranium deposit, Kiggavik, Nunavut, Canada. Mineralium Deposita 52, 211-232.
13. Dare S.A.S., Barnes S.J., Beaudoin G., Méric J., Boutroy E., Potvin-Doucet C., 2014. Trace elements in magnetite as petrogenetic indicators. Mineralium Deposita, 49, 785-796.
14. Dupuis C., and Beaudoin G., 2011. Discriminant diagrams for iron oxide trace element fingerprinting

of mineral deposit types. Mineralium Deposita, 46 (4), 319-335.

15. Dyke A.S., 2004. An outline of North American deglaciation with emphasis on central and northern Canada; In: Quaternary Glaciations. Extent and Chronology Part II- 2004, (ed.) K. Ehlers and P.L. Gibbard; Elsevier, Amsterdam, 373-424.
16. Dyke A.S., Andrews J.T., Clark P.U., England J.H., Miller G.H., Shaw J., Veillette J.J., 2002. The Laurentide and Innuitian ice sheets during the Last Glacial Maximum. Quaternary Science Reviews 21, 9-31.
17. Fandrich R., Gu Y., Burrows D., Moeller K., 2007. Modern SEM-based mineral liberation analysis. International Journal of Mineral Processing, 84 (1-4), 310-320.
18. Farkas A., 1984. Mineralogy and host rock alteration of the Lone Gull deposit: Urangesellschaft internal report, 44 pages.
19. Fayek M., Quirt D., Jefferson C.W., Camacho A., Ashcroft G., Shabaga B., Sharpe R., 2017. The Kiggavik-Andrew Lake structural trend uranium deposits: an overview. In SGA Extended Abstract proceedings. SGA 2017 Conference Quebec City, August 20-23. In press.
20. Flood R.P., Orford J.D., McKinley J.M., Roberson S., 2015. Effective grain size distribution analysis for interpretation of tidal–deltaic facies: West Bengal Sundarbans. Sedimentary Geology, 318, 58-74.
21. Fuchs H.D., and Hilger W., 1989. Kiggavik (Lone Gull): An unconformity related uranium deposit in the Thelon Basin, Northwest Territories, Canada. IAEA TECDOC 500, 429-455.
22. Fuchs H.D., Hilger W., Prosser E., 1985. Geology and exploration history of the Lone Gull property. In: Uranium Deposits of Canada, (ed.) E.L. Evans; Canadian Institute of Mining and Metallurgy 33, 286-292.
23. Gall Q., Peterson T.D., Donaldson J.A., 1992. A proposed revision of early Proterozoic stratigraphy of the Thelon and Baker Lake basins, Northwest Territories. Geological Survey of Canada, Current Research Paper 92-01C, 129-137.
24. Geladi P., and Grahn H., 1996. Multivariate Image Analysis. John Wiley & Sons, 330 pages.
25. Geladi P., Isaksson H., Lindqvist L., Wold S., Esbensen K., 1989. Principal component analysis of multivariate images. Chemometrics and Intelligent Laboratory Systems 5 (3), 209-220.
26. Grare, A., Benedicto, A, Lacombe, O., Trave, A., Ledru, P., Blain, M., and Robbins, J., 2018. The Contact uranium prospect, Kiggavik project, Nunavut (Canada): Tectonic history, structural constraints and timing of mineralization. Ore Geology Reviews, v. 93, p. 141–167.
27. Hiatt E. E., Kyser K., Dalrymple R.W., 2003. Relationships among sedimentology, stratigraphy, and diagenesis in the Proterozoic Thelon Basin, Nunavut, Canada: Implications for paleoaquifers and sedimentary-hosted mineral deposits. Journal of Geochemical Exploration, 80 (2-3), 221-240.
28. Hiatt E.E., Palmer S.E., Kyser T.K., O'Connor T.K., 2010. Basin evolution, diagenesis and uranium mineralization in the Paleoproterozic Thelon basin, Nunavut, Canada. Basin Research, 22, 302-323.
29. Hoffman P.F., 1988. United plates of America, the birth of a craton: Early Proterozoic assembly and growth of Laurentia. Annual Review of Earth and Planetary Sciences, 16, 543-603.
30. Jefferson C.W., Thomas D.J., Gandhi S.S., Ramaekers P., Delaney G., Brisbin D., Cutts C., Quirt D., Portella P., Olson R.A., 2007. Unconformity-associated uranium deposits of the Athabasca Basin, Saskatchewan and Alberta. Goodfellow W.D., (ed.), Mineral Deposits of Canada, Geological Association of Canada, Mineral Deposits Division, Special Publication No. 5, 273-305.
31. Johnstone D., Bethune K.M., Quirt D., 2016. Lithostratigraphic and structural controls of uranium mineralization in the Kiggavik East, Centre and Main Zone deposits, Nunavut. In: Abstracts-Résumés, Geological Association of Canada - Mineralogical Association of Canada, Joint Annual Meeting, Whitehorse Yukon, 1-3 June 2016, v. 39, p. 41.
32. Johnstone, D., Bethune, K., Quirt, D., Benedicto, A., and Ledru, P., 2017. Lithostructural controls of U mineralization in the Kiggavik Main and Centre zones, north-central Rae craton: A record of long-

lived tectonism and ground preparation for U ore systems. In: Abstracts-Résumés, Geological Association of Canada - Mineralogical Association of Canada, Joint Annual Meeting, Kingston Ontario, 14-18 May 2017, v. 40, p. 190.

33. Kaminsky F.V., and Belousova E.A., 2009. Manganoan ilmenite as kimberlite/diamond indicator mineral. Russian Geology and Geophysics, 50 (12), 1212-1220.
34. LeCheminant A.N., Miller A.R., Booth G.W., Murray M.J., Jenner G.A., 1979. Geology of the Tebesjuak Lake map area: A progress report with notes on uranium and base metal mineralization. Geological survey of Canada, Open File 663, 26 pages.
35. Mackay D.A.R., Simandl G.J., Ma W., Gravel J., Redfearn M., 2015. Indicator minerals in exploration for specialty metal deposits: A QEMSCAN® approach. Symposium on critical and strategic materials. British Columbia Geological Survey, Paper 2015-3, 2011-2017.
36. Makvandi S., Beaudoin G., McClenaghan M.B., Layton-Matthews D., 2015. The surface texture and morphology of magnetite from the Izok Lake volcanogenic massive sulfide deposit and local glacial sediments, Nunavut, Canada: Application to mineral exploration. Geochemical Exploration, 150, 84-103.
37. Makvandi S., Beaudoin G., McClenaghan M.B., Layton-Matthews D., 2016b. Principal component analysis of Mineral Liberation Analysis data on angularity, size distribution and mineral associations of magnetite and hematite from the Izok Lake VMS deposit (Nunavut, Canada) and local till. The GAC-MAC Conference 2016, June 1-3, 2016, in Whitehorse, Canada.
38. Makvandi S., Beaudoin G., McClenaghan M.B., Quirt D., 2017. Geochemistry of magnetite and hematite from bedrock and local till at the Kiggavik uranium deposit: Implications for sediment provenance. Journal of Geochemical Exploration, 183, 1-21.
39. Makvandi S., Beaudoin G., Quirt D., Ledru P., Fayek M., 2018. Trace element geochemistry of Fe-(hydro)oxides from the unconformity-related U deposits in the Kiggavik camp (Nunavut, Canada). RFG2018, Vancouver, BC, Canada, 18-21 June 2018.
40. Makvandi S., Ghasemzadeh-Barvarz M., Beaudoin G., Grunsky E.C., McClenaghan B.M., Duchesne C. 2016a. Principal component analysis of magnetite composition from volcanogenic massive sulfide deposits: Case studies from the Izok Lake (Nunavut, Canada) and Halfmile Lake (New Brunswick, Canada) deposits. Ore Geology Reviews, 72, 60-85.
41. Makvandi S., Ghasemzadeh-Barvarz M., Beaudoin G., Grunsky E.C., McClenaghan B.M., Duchesne C., Boutroy E., 2016c. Partial least squares-discriminant analysis of trace element compositions of magnetite from various VMS deposit subtypes: Application to mineral exploration. Ore Geology Reviews, 78, 388-408.
42. McClenaghan M.B. 2011. Overview of common processing methods for recovery of indicator minerals from sediment and bedrock. Geochemistry: Exploration, Environment, Analysis, 11, 265-278.
43. McClenaghan, M.B. and Kjarsgaard, B.A. 2007. Indicator mineral and surficial geochemical exploration methods for kimberlite in glaciated terrain, examples from Canada. In Mineral Resources of Canada: A Synthesis of Major Deposit-types, District Metallogeny, the Evolution of Geological Provinces and Exploration Methods, (ed.) W.D. Goodfellow, Geological Association of Canada, Special Publication No. 5, p. 983-1006.
44. McClenaghan, M.B. and Paulen, R.C. 2017. Mineral Exploration in Glaciated Terrain. In: Menzies, J. and van der Meer, J.J-M. (eds) Past Glacial Environments (Sediments, Forms and Techniques) A new & revised edition, Elsevier, p. 689-751.
45. McClenaghan M.B., Hicken A.K., Averill S.A., Paulen R.C., Layton-Matthews D., 2012. Indicator mineral abundance data for bedrock and till samples from the Izok Lake Zn-Cu-Pb-Ag Volcanogenic Massive Sulphide Deposit, Nunavut. Geological Survey of Canada, Open File 7075.

46. McClenaghan, M.B., Paulen, R.C., Layton-Matthews, D., Hicken, A.K. and Averill, S.A. 2015. Glacial dispersal of gahnite from the Izok Lake Zn-Cu-Pb-Ag VMS deposit, northern Canada. Geochemistry: Exploration, Environment, Analysis, 15, 333-349.
47. McMartin I., and Dredge L.A., 2005. History of ice flow in the Schultz Lake (NTS 66a) and Wager Bay (NTS 56G) areas, Kivalliq Region, Nunavut. Geological Survey of Canada, Current Research, 2005-B-2.
48. McMartin I., and Henderson P.J., 2004. Evidence from Keewatin (central Nunavut) for paleo-ice divide migration; Géographie physique et Quaternaire, 58, 163-186.
49. McMartin I., Dredge L.A., Ford K.L., Kjarsgaard I.M., 2006. Till composition, provenance and stratigraphy beneath the Keewatin Ice Divide, Schultz Lake area (NTS 66A), mainland Nunavut. Geological Survey of Canada, Open File 5312.
50. Miller A.R., and Peterson T.D. 2015. Geology and petrology of the Schultz Lake Intrusive Complex and its relationship to unconformity uranium deposits: Schultz Lake, NTS 66A/5 and Aberdeen Lake, 66B/8, Western Churchill Province. Geological Survey of Canada, Open File 7858.
51. Nadoll P., Angerer T., Mauk J.L., French D., Walshe J., 2014. The chemistry of hydrothermal magnetite: A review. Ore Geology Reviews, 61, 1-32.
52. Peterson T.D., Scott J.M.J., LeCheminant A.N., Jefferson C.W., Pehrsson S.J., 2015. The Kivalliq Igneous Suite: Anorogenic bimodal magmatism at 1.75 Ga in the western Churchill Province, Canada. Precambrian Research 262, 101-119.
53. Pehrsson S.J., Berman R., Davis W.J., 2013. Paleoproterozoic orogenesis during Nuna aggregation: a case study of reworking of the Archean Rae craton, Woodburn Lake, Nunavut. Precambrian Research 232, 167-188.
54. O'Brien J.J., Spry P.G., Teale G.S., Jackson S.E., Koenig A.E., 2015. Gahnite composition as a means to fingerprint metamorphosed massive sulfide and non-sulfide zinc deposits. Journal of Geochemical Exploration 159, 48-61.
55. Quirt D. 2017. Clay mineral host-rock alteration at the Bong basement-hosted uranium deposit, Kiggavik area, Nunavut. In SGA Extended Abstract proceedings. SGA 2017 Conference Quebec City, August 20-23. In press.
56. Rainbird R.H., and Davis W.J., 2007. U-Pb detrital zircon geochronology and provenance of the late Paleoproterozoic Dubawnt Supergroup: Linking sedimentation with tectonic reworking of the western Churchill province, Canada. Geological Society of America Bulletin, 119, 314-328.
57. Rainbird R.H., Hadlari T., Aspler L.B., Donaldson J.A., LeCheminant A.N., Peterson T.D., 2003. Sequence stratigraphy and evolution of the Paleoproterozoic intracontinental Baker Lake and Thelon basins, western Churchill Province, Nunavut, Canada. Precambrian Research, 125, 21-53.
58. Riegler T., Lescuyer J.L., Wollenberg P., Quirt D., Beaufort D., 2014. Alteration related to uranium deposits in the Kiggavik-Andrew Lake Structural Trend, Nunavut, Canada: New insights from petrography and clay mineralogy. The Canadian Mineralogist, 52, 27-45.
59. Riegler T., Beaufort M.-F., Allard T., Pierson-Wickmann A.C., Beaufort D., 2016a. Nanoscale relationships between uranium and carbonaceous material in alteration halos around unconformity-related uranium deposits of the Kiggavik camp, Paleoproterozoic Thelon Basin, Nunavut, Canada. Ore Geology Review 79, 382-391.
60. Riegler T., Quirt D., Beaufort D., 2016b. Spatial distribution and compositional variation of APS minerals related to uranium deposits in the Kiggavik-Andrew Lake structural trend, Nunavut, Canada. Mineralium Deposita 51, 219-236.
61. Robinson S.V.J., Jefferson C.W., Paulen R.C., Layton-Matthews D., Joy B., Quirt D., 2016. Till and bedrock heavy mineral signatures of the Kiggavik uranium deposits, Nunavut. Geological Survey of Canada, Open File 7771.

62. Robinson S.V.J., Paulen R.C., Jefferson C.W., McClenaghan M.B., Layton-Matthews D., Quirt D., Wollenberg P., 2014. Till geochemical signatures of the Kiggavik uranium deposit, Nunavut. Geological Survey of Canada, Open File 7550.
63. Rudashevsky N.S., Garuti G, Anderson J.C.O., Krester Y.L., Rudashevsky V.N., Zaccarini F., 2002. Separation of accessory minerals from rocks and ores by hydroseparation (HS) technology: method and application to CHR-2 chromitite, Niquelandia intrusion, Brazil. Applied Earth Science: IMM Transactions section B 111, 87-94.
64. Scott J.M.J., Peterson T.D., Davis W.J., Jefferson C.W., Cousens B.L., 2015. Petrology and geochronology of Paleoproterozoic intrusive rocks, Kiggavik uranium camp, Nunavut; Canadian Journal of Earth Sciences, 52, 495-518.
65. Shabaga B.M., Fayek M., Quirt D., Jefferson C.W., Camacho A., 2017. Mineralogy, geochronology, and genesis of the Andrew Lake uranium deposit, Thelon Basin, Nunavut, Canada. Canadian Journal of Earth Sciences, 54, 850-868.
66. Sharpe R., Fayek M., Quirt D., Jefferson C.W., 2015. Geochronology and genesis of the Bong uranium deposit, Thelon Basin, Nunavut, Canada. Economic Geology, 110, 1759-1777.
67. Suk M., 2013. Petrology of metamorphic rocks. Elsevier, 232 pages.
68. Sylvester P.J., 2012. Chapter 1: Use of the Mineral Liberation Analyzer (MLA) for mineralogical studies of sediments and sedimentary rocks. Mineralogical Association of Canada, Short Course 42, St. John's, NL, 1-16.
69. Tschirhart V., Morris W.A., Jefferson C.W. 2013. Framework geophysical modelling of granitoid vs. supracrustal basement to the northeast Thelon Basin around the Kiggavik uranium camp, Nunavut. Canadian Journal of Earth Sciences, 50, 667-677.
70. Tschirhart, V., Morris, W.A., Jefferson, C.W. 2014. Unconformity surface architecture of the northeast Thelon Basin, Nunavut, derived from integration of magnetic source depth estimates [online]. Society of Exploration Geophysicists and American Association of Petroleum Geologists, 2: SJ263-SJ278.
71. Wishart D., 2013. Module 6- Backgrounder in Statistical Methods. Informatics and Statistics for Metabolomics Workshop 2013, Toronto, Canada (53 pages).
72. Zaleski E., Pehrsson S., Duke N., Davis W.J., L'Heureux R., Greiner E., Kerswill J.A., 2000. Quartzite sequences and their relationships, Woodburn Lake group, western Churchill Province, Nunavut. Geological Survey of Canada, Current Research (Online) no. 2000-C7, 10 pages.

Table 1. A) Bedrock and B) till samples description.

A

Sample ID	Rock type	Easting*	Northing	Lithology	Mineralogy
10-PTA-R018**	Quartz arenite	553695	7152777	Thelon Formation	Quartz (83%), alkaline feldspar (15%), hematite (2%)
10-PTA-R020**	Quartz arenite	555263	7151994	Thelon Formation	Quartz (90%), pseudomorphs feldspar (6%), hematite (3%), goethite (<1%), ilmenite (tr.)
10-PTA-R009**	Martell syenite	565130	7146834	Hudson Suite Intrusive	Alkaline feldspar (45%), quartz (5%), plagioclase (25%), biotite (5%), phologopite (5%), muscovite (2%), chlorite (7%), pyrite (1%), hematite (1%), magnetite (1%), ilmenite (<1%), apatite (1%), zircon (<1%)
10-PTA-R060	Leucogranite	565340	7146959	Hudson Granite and possibly Nueltin Granite	Alkalie feldspar (43%), quartz (40%), hornblende (5%), biotite (5%), muscovite (3%), magnetite (1%), hematite (<1%), ilmenite and sphene (1%), zircon and apatite (1%), pyrite (tr.)
10-PTA-R041	Granite	564968	7146879	Lone Gull plug: Hudson + Nueltin	Alkali feldspar (40%), quartz (30%), plagioclase (20%), muscovite (7%), chlorite (1%), magnetite (1%), zircon (tr), pyrite (tr.), molybdenite (tr.)
10-PTA-R026a	Mafic syenite	552112	7142563	Hudson Igneous Suite	Alkaline feldspar (28%), amphibole (20%; more horblende and less actinolite), plagioclase (15%), clinopyroxene (15%), biotite (10%), quartz (5%), magnetite (3%), hematite (1%), apatite (1%), pyrite (1%), chalcopyrite (1%)
10-PTA-R054	Quartzite	564877	7146889	Lower Ketyet River Group	Quartz (93%), muscovite (5%), hematite (<2%), magnetite (tr.)
10-PTA-R140**	Epiclastic	565807	7147336	Pukiq Lake Formation	Quartz (45%), clay alteration (25%), alkaline feldspar (15%), muscovite and sericite (15%), hematite (5%)

Sample name	Easting	Northing	Location & direction from the Main Zone	Distance from Main Zone
10-PTA-135	570008	7147566	up ice, NE	5 km
10-PTA-117	565154	7146913	overlying	10 m
10-PTA-096	563729	7147964	down ice, NW	2 km
10-PTA-101	564338	7147064	down ice, WNW	1 km

	10-PTA-104	564796	7147744	down ice, NW	1 km
B					
	10-PTA-112	564694	7146983	down ice, WNW	500 m
	10-PTA-115	565045	7146933	down ice, WNW	50 m
	10-PTA-124	564899	7146933	down ice, WNW	250 m
	10-PTA-128	564900	7147365	down ice, NW	500 m
	10-PTA-130	565024	7147155	down ice, NW	250 m

* For all bedrock and till samples: DATUM 83, Zone 14N.

** Fe oxide grains in the polished thin sections made of these samples' offcuts were investigated in this study.

Figure Captions

Figure 1. A) The location of **B** in Canada. **B)** Simplified regional geology of the western Churchill Province and surrounding area around the Athabasca and Thelon basins, and location of the Kiggavik camp in the north east of the Thelon Basin, Nunavut, Canada (modified after Renac et al., 2002). Red box represents location of Fig. 2 (studied area).

Figure 2. A) Regional bedrock geology map of the Kiggavik area (modified from Riegler et al. 2014; Scott et al. 2015; Sharpe et al. 2015, Shabaga et al., 2017) showing the location of the Kiggavik deposits. B) Simplified stratigraphic column of lithological and intrusive units in the Western Churchill Province (modified after Peterson et al., 2015; Grare et al., 2018). C) Kiggavik Bedrock and till samples location. Note all rock sample numbers have the prefix 10-PTA- (e.g., R018 refers to sample 10-PTA-R018). In till sample numbers, T replaced the prefix (e.g., T128 refers to sample 10-PTA-128).

Figure 3. A selection of SEM backscatter images showing mineral aggregates from the Kiggavik igneous, metasedimentary, and sedimentary bedrock lithologies. **A)** A fractured magnetite (Mag) grain from the Hudson and Kivalliq Suites granite. **B)** A mineral aggregate from the Hudson Igneous Suite (HIS) mafic syenite consisting of magnetite and hornblende (Hbl). Hornblende replaced magnetite along edges and fractures. **C)** Pseudomorph hematite (Hem) after magnetite from the Hudson and Kivalliq Suites granite associated with clay alteration. Zircon (Zrn) occurs as inclusions in Fe oxides. **D)** Specular hematite from Ketyet River Group quartzite is associated with quartz and partly replaced magnetite. **E)** Detrital hematite in association with quartz (Qz) and clay from Snow Island Suite (SIS) epiclastic rocks. **F)** Round hematite grain from Thelon Formation quartz arenite intergrown with two quartz phases (Qz1 & Qz2).

Figure 4. A selection of SEM backscatter images showing mineral aggregates including Fe oxides from Kiggavik till. **A)** Polymineralic aggregate from the 0.25-0.5 mm fraction of till sample

10-PTA-130 including magnetite, quartz and garnet (Grn) altered by needles of hematite. **B)** Polymineralic aggregate from the 0.5-2.0 mm fraction of till sample 10-PTA-101 including magnetite interlocked with ilmenite (Ilm) and mafic minerals such orthopyroxene (Opx) and clinopyroxene (Cpx). **C)** Polymineralic aggregate from the 0.25-0.5 mm fraction of till sample 10-PTA-096, consisting of magnetite, quartz, and apatite (Ap). **D)** Polymineralic aggregate from the 0.5-2.0 mm fraction of till sample 10-PTA-096 including disseminated magnetite with plagioclase (Pl) inclusions, and slightly replaced by titanite (Ttn). **E)** Hematite pseudomorph consisting of orthoclase (Or) micro-inclusions and altered by clays from the 0.5-2.0 mm fraction of till sample 10-PTA-104. **F)** Round shape hematite from the 0.25-0.5 mm fraction of till sample 10-PTA-096 characterized by pyrite (Py) inclusions and altered by quartz from edges.

Figure 5. Mineral liberation analysis (MLA) false color images. **A)** Liberated Fe oxide grain from the 0.25-0.5 mm fraction of till sample 10-PTA-101. **B)** Magnetite aggregate from the 0.5-2.0 mm fraction of till sample 10-PTA-117 composed of different mineral inclusions such as titanomagnetite (TitanoMag), spinel (Spl), chlorite (Chl), quartz (Qz), zeolite (Zeo), hornblende (Hbl), gahnite (Ghn), and grunerite (Gru). **C)** Fine-grained mineral components of a polymineralic aggregate from the 0.5-2.0 mm fraction of till sample 10-PTA-135. The aggregate is composed of Fe oxides (Hem/Mag), clay minerals, quartz, zeolite, chromite (Chr), biotite (Bi), hornblende, chlorite, orthoclase (Or), plagioclase (Pl), Cr-rich magnetite (Cr-Mag), epidote (Ep), and apatite (Ap). In this aggregate, Fe oxides occur as inclusions in clay minerals.

Figure 6) Principal component analysis (PCA) of integrated data of grain size and mineral association of Fe oxides from the Kiggavik bedrock samples. Loadings (PC1-PC2) and scores (t_1-t_2) of the first and second principal components are shown in **A** and **B**, respectively. PCA loadings show correlations among different variables and the impact of these correlations on the distribution/classification of the Kiggavik bedrock samples in the scores scatter plot. The red numbers in **A** represent different grain size classes. ***Abbreviations***- St: staurolite; Grn: garnet; Opx:

orthopyroxene; Chl: chlorite; Bi: biotite; Or: orthoclase; Zeo: zeolite; Ms: muscovite; Cpx: clinopyroxene; Cal: calcite; Rt: rutile; Ttn: titanite; Spl: spinel; Zrn: zircon; Ab: albite; An: anorthite; Lm: limonite; TitanoMag: titano-magnetite; Ilm: ilmenite; Qz: quartz; Ep: epidote; Ap: apatite; Hbl: hornblende; Gru: grunerite; Sulf: sulfides; Ghn: gahnite; Chr: chromite; Cr-Mag: Cr-rich magnetite.

Figure 7) Principal component analysis (PCA) of integrated data of grain size and mineral association of Fe oxides from the 0.25-0.5 mm and 0.5-2.0 mm fractions of the Kiggavik till samples. Loadings (PC1-PC2) and scores (t_1-t_2) of the first and second principal components are shown in **A** and **B**, respectively. PCA loadings show correlations among different variables and the impact of these correlations on the distribution/classification of different fractions of the Kiggavik till samples in the scores scatter plot. The red numbers in **A** represent different grain size classes. Abbreviations for mineral names are the same as in Fig. 6.

Figure 8. Principal component analysis (PCA) of integrated data of grain size and mineral association of Fe oxides from the Kiggavik bedrock and till samples. Loadings (PC1-PC2) and scores (t_1-t_2) of the first and second principal components are shown in **A** and **B**, respectively. The red numbers in **A** represent different grain size classes. Abbreviations for mineral names are the same as in Fig. 6.

Figure 9. Principal component analysis (PCA) of trace elements concentration in Fe oxides from the Kiggavik bedrock and till samples. Loadings (PC1-PC2) and scores (t_1-t_2) of the first and second principal components are shown in **A** and **B**, respectively.

Figure 10. Principal component analysis (PCA) compares the grain size, and the abundance of minerals in association with Fe oxides from the Kiggavik bedrock and till samples with Fe oxides MLA data from bedrocks and till from the Izok Lake and Halfmile VMS deposits areas. Loadings (PC1-PC2) and scores (t_1-t_2) of the first and second principal components are shown in **A** and **B**, respectively. The red numbers in **A** represent different grain size classes. ***Abbreviations***- Zrn: zircon;

Cal: calcite; Rt: rutile; Ttn: titanite; Ab: albite; Ilm: imenite; TitanoMag: titano-magnetite; Or: orthoclase; Ms: muscovite; Sulf: suflides: Px: Pyroxene; Ax: axinite; Ghn: gahnite; Crn: corundum; Bi: biotite; St: staurolie; An: anorthite; Zeo: zeolite; Amp: amphiboles; Chr: chromite; Cr-Mag: Cr-rich magnetite; Ep: epidote; Grn: garnet; Spl: spinel; Ap: apatite; Qz: quartzite; Lm: limonite; Chl: chlorite.

Highlights

PCA of MLA data to classify the source of Fe-oxides in Kiggavik till

Fe-oxide grain size and mineral association as exploration tools

Differentiating between different geologic setting using Fe-oxides MLA data

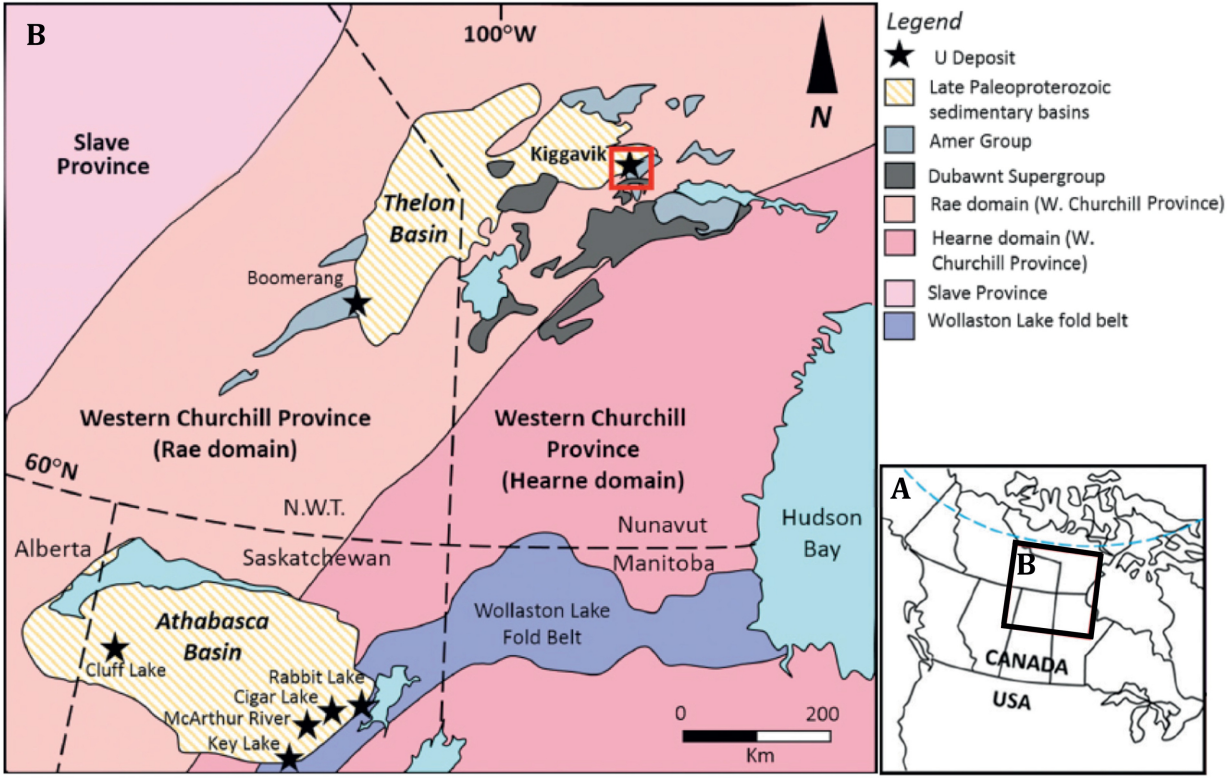
B
100°W
N
Slave Province
Kiggavik
Thelon Basin
Boomerang
Western Churchill Province (Rae domain)
Western Churchill Province (Hearne domain)
60°N
N.W.T.
Nunavut
Alberta
Saskatchewan
Manitoba
Hudson Bay
Athabasca Basin
Cluff Lake
Rabbit Lake
Cigar Lake
McArthur River
Key Lake
Wollaston Lake Fold Belt
0
200
Km
Legend
U Deposit
Late Paleoproterozoic sedimentary basins
Amer Group
Dubawnt Supergroup
Rae domain (W. Churchill Province)
Hearne domain (W. Churchill Province)
Slave Province
Wollaston Lake fold belt
A
B
CANADA
USA

Figure 1

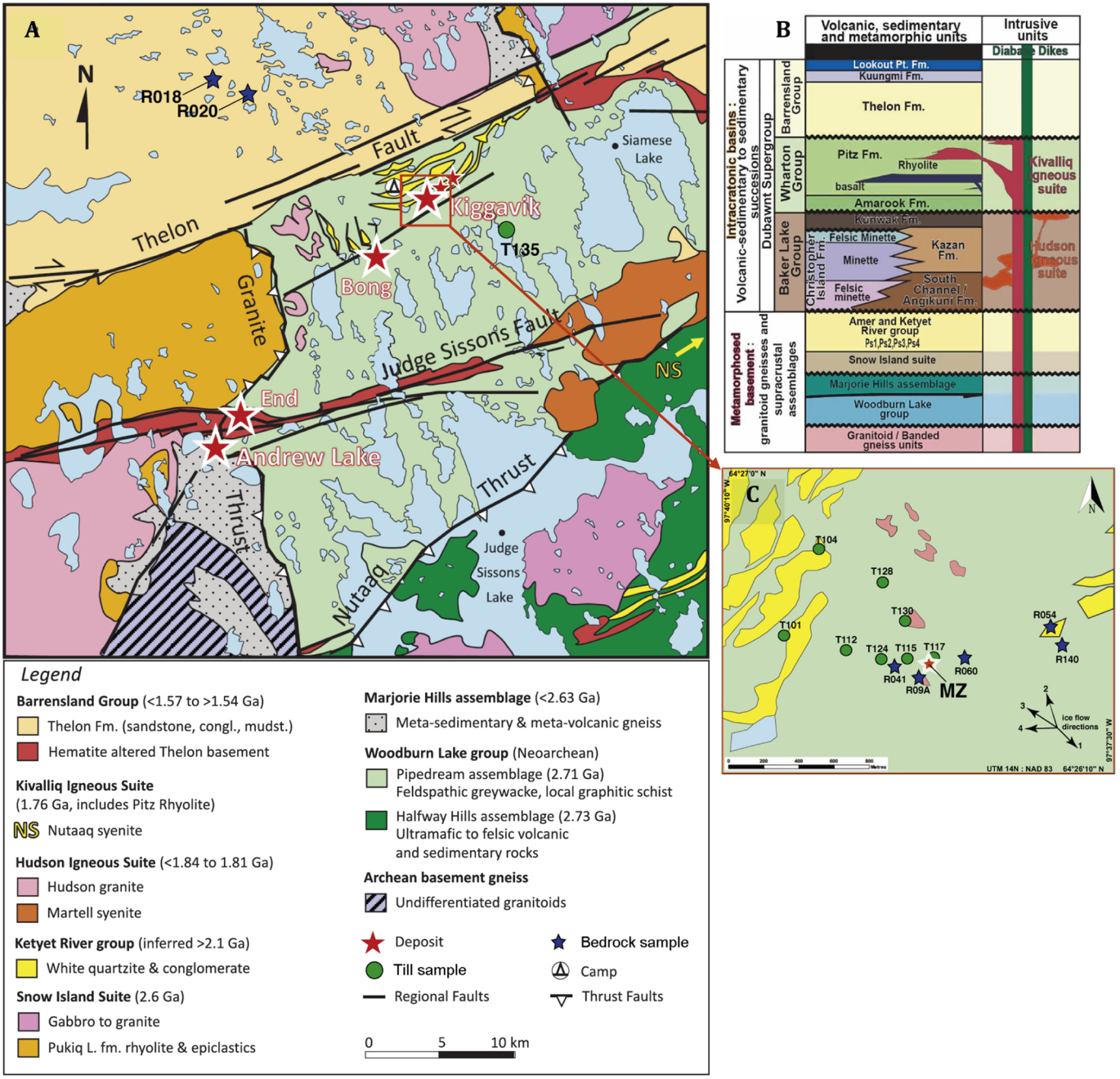
A
N
R018
R020
Fault
Thelon
Granite
Siamese Lake
Kiggavik
T135
Bong
Judge Sissons Fault
NS
End
Andrew Lake
Thrust
Thrust
Judge Sissons Lake
Nutaaq
B
Volcanic, sedimentary and metamorphic units
Intrusive units
Diabase Dikes
Intracratonic basins : Volcanic-sedimentary to sedimentary succesions
Dubawnt Supergroup
Barrensland Group
Lookout Pt. Fm.
Kuungmi Fm.
Thelon Fm.
Wharton Group
Pitz Fm.
Rhyolite
basalt
Amarook Fm.
Baker Lake Group
Kunwak Fm.
Christopher Island Fm.
Felsic Minette
Minette
Felsic minette
Kazan Fm.
South Channel / Angikuni Fm.
Kivalliq Igneous suite
Hudson Igneous suite
Metamorphosed basement : granitoid gneisses and supracrustal assemblages
Amer and Ketyet River group
Ps1,Ps2,Ps3,Ps4
Snow Island suite
Marjorie Hills assemblage
Woodburn Lake group
Granitoid / Banded gneiss units
C
64°27'0" N
97°40'10" W
T104
T128
T130
T101
T112
T124
T115
T117
R054
R140
R060
R041
R09A
MZ
ice flow directions
97°37'30" W
UTM 14N : NAD 83
64°26'10" N
Legend
Barrensland Group (<1.57 to >1.54 Ga)
Thelon Fm. (sandstone, congl., mudst.)
Hematite altered Thelon basement
Kivalliq Igneous Suite
(1.76 Ga, includes Pitz Rhyolite)
NS Nutaaq syenite
Hudson Igneous Suite (<1.84 to 1.81 Ga)
Hudson granite
Martell syenite
Ketyet River group (inferred >2.1 Ga)
White quartzite & conglomerate
Snow Island Suite (2.6 Ga)
Gabbro to granite
Pukiq L. fm. rhyolite & epiclastics
Marjorie Hills assemblage (<2.63 Ga)
Meta-sedimentary & meta-volcanic gneiss
Woodburn Lake group (Neoarchean)
Pipedream assemblage (2.71 Ga)
Feldspathic greywacke, local graphitic schist
Halfway Hills assemblage (2.73 Ga)
Ultramafic to felsic volcanic and sedimentary rocks
Archean basement gneiss
Undifferentiated granitoids
Deposit
Bedrock sample
Till sample
Camp
Regional Faults
Thrust Faults
0 5 10 km

Figure 2

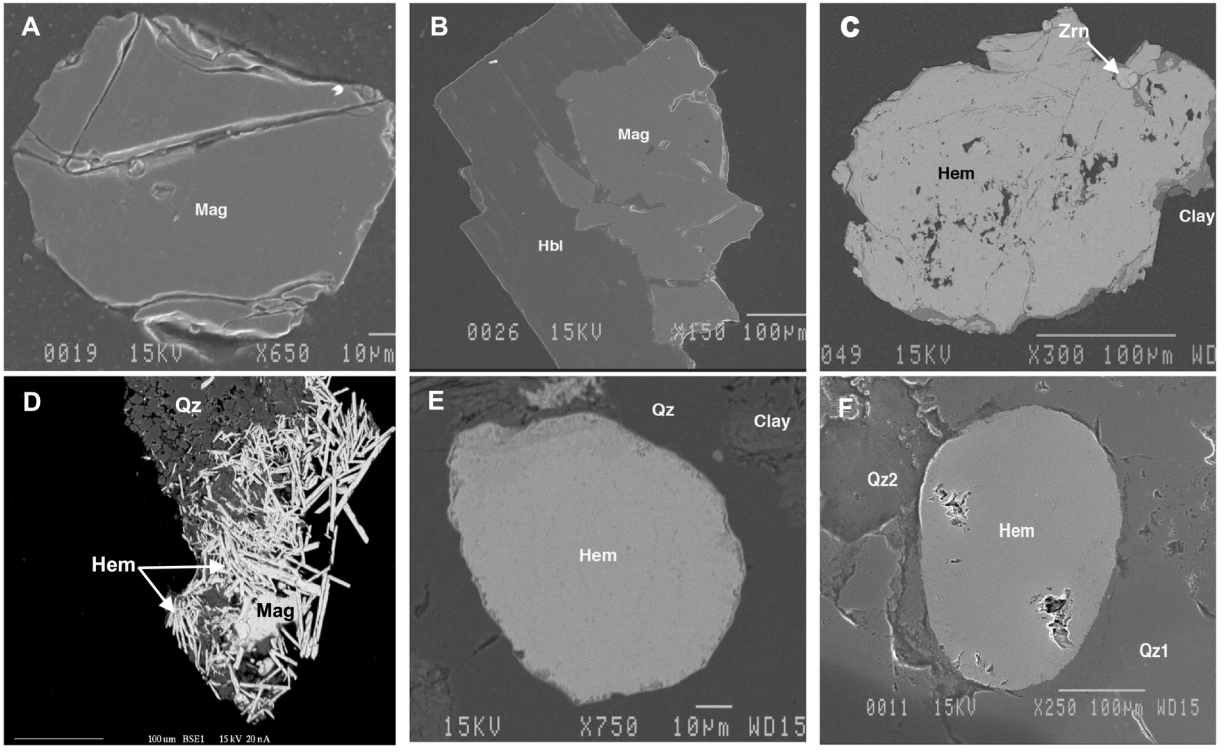
A
Mag
0019 15KV X650 10µm
B
Mag
Hbl
0026 15KV X150 100µm
C
Zrn
Hem
Clay
049 15KV X300 100µm WD
D
Qz
Hem
Mag
100um BSE1 15kV 20nA
E
Qz
Clay
Hem
15KV X750 10µm WD15
F
Qz2
Hem
Qz1
0011 15KV X250 100µm WD15

Figure 3

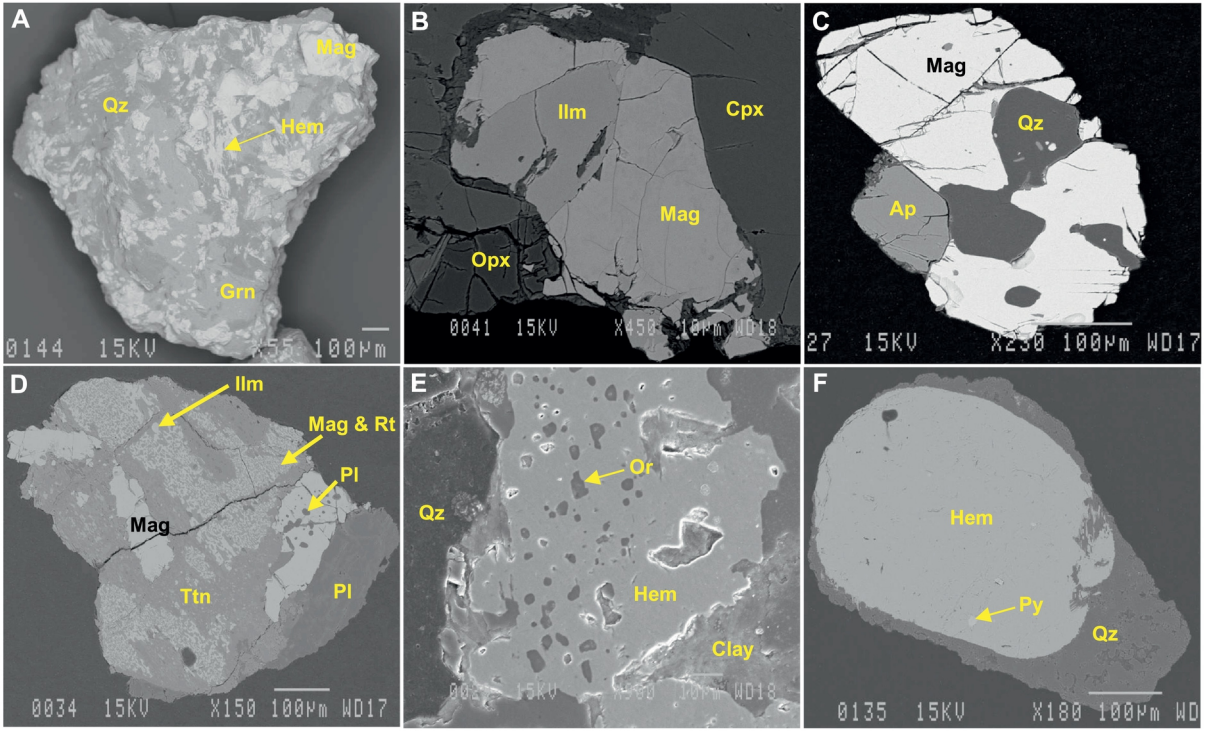
A
Mag
Qz
Hem
Grn
0144 15KV X55 100µm
B
Ilm
Cpx
Mag
Opx
0041 15KV X450 10µm WD18
C
Mag
Qz
Ap
27 15KV X250 100µm WD17
D
Ilm
Mag & Rt
Pl
Mag
Ttn
Pl
0034 15KV X150 100µm WD17
E
Or
Qz
Hem
Clay
F
Hem
Py
Qz
0135 15KV X180 100µm WD

Figure 4

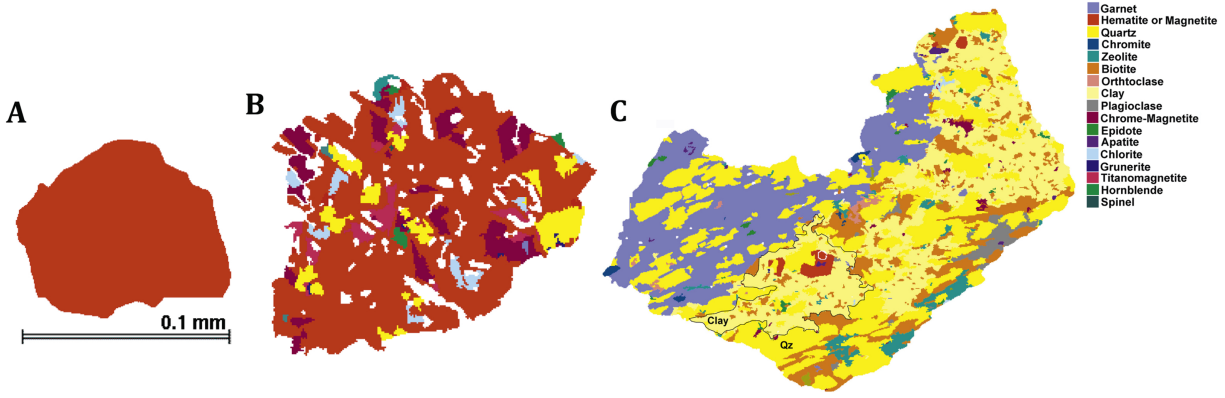
A
0.1 mm
B
C
Clay
Qz
Garnet
Hematite or Magnetite
Quartz
Chromite
Zeolite
Biotite
Orthtoclase
Clay
Plagioclase
Chrome-Magnetite
Epidote
Apatite
Chlorite
Grunerite
Titanomagnetite
Hornblende
Spinel

Figure 5

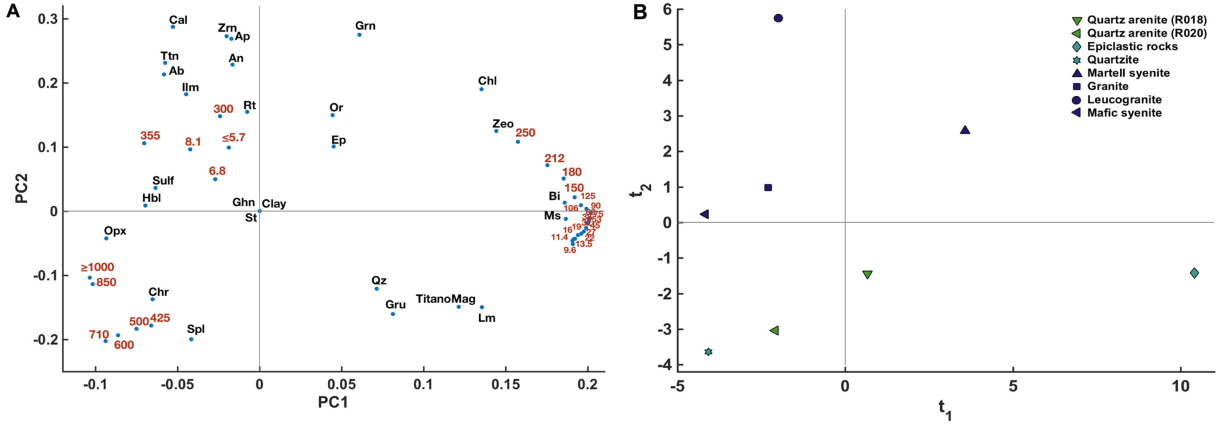
A
PC2
PC1
Cal
Zm
Ap
An
Ttn
Ab
Ilm
300
Rt
355
8.1
≤5.7
6.8
Sulf
Hbl
Ghn
Clay
St
Opx
≥1000
850
Chr
500
425
710
600
Spl
Grn
Or
Ep
Chl
Zeo
250
212
180
150
125
Bi
Ms
Qz
Gru
TitanoMag
Lm
B
t_2
t_1
Quartz arenite (R018)
Quartz arenite (R020)
Epiclastic rocks
Quartzite
Martell syenite
Granite
Leucogranite
Mafic syenite

Figure 6

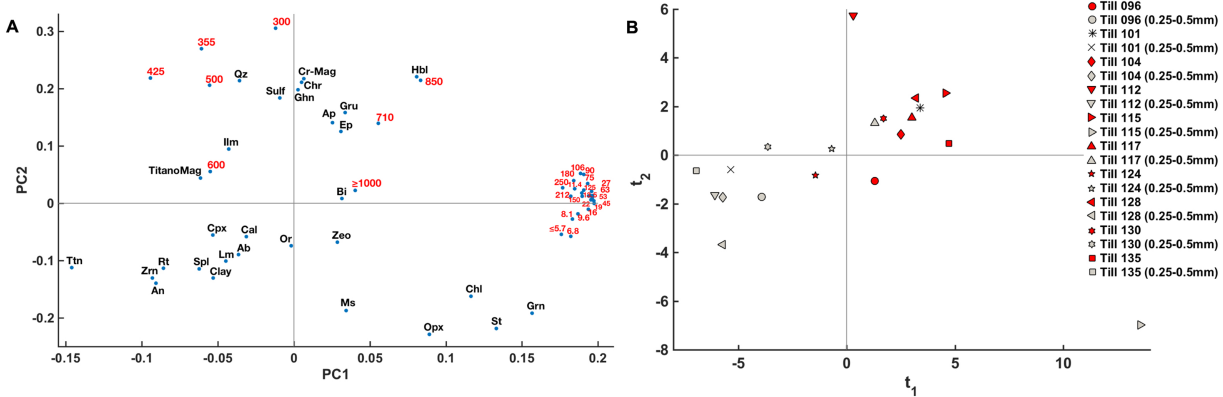
A
PC2
PC1
300
355
425
500
Qz
Cr-Mag
Chr
Sulf
Ghn
Hbl
850
Gru
Ap
Ep
710
Ilm
TitanoMag
600
≥1000
Bi
Cpx
Cal
Or
Zeo
Ab
Lm
Ttn
Rt
Spl
Zm
Clay
An
Chl
Ms
Grn
Opx
St
B
t2
t1
Till 096
Till 096 (0.25-0.5mm)
Till 101
Till 101 (0.25-0.5mm)
Till 104
Till 104 (0.25-0.5mm)
Till 112
Till 112 (0.25-0.5mm)
Till 115
Till 115 (0.25-0.5mm)
Till 117
Till 117 (0.25-0.5mm)
Till 124
Till 124 (0.25-0.5mm)
Till 128
Till 128 (0.25-0.5mm)
Till 130
Till 130 (0.25-0.5mm)
Till 135
Till 135 (0.25-0.5mm)

Figure 7

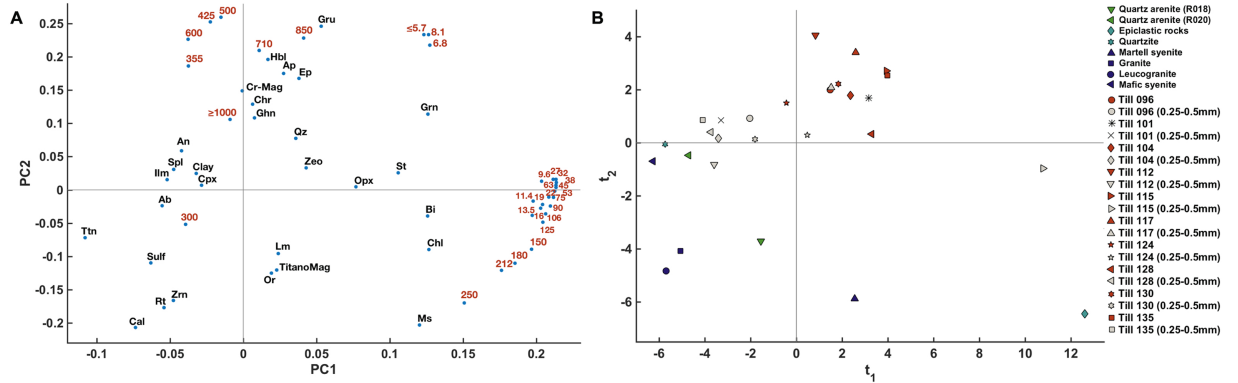
A
PC2
PC1
425
500
600
355
710
850
Gru
≤5.7
8.1
6.8
Hbl
Ap
Ep
Cr-Mag
Chr
Ghn
≥1000
Grn
An
Spl
Ilm
Clay
Cpx
Oz
Zeo
St
Opx
Ab
300
Ttn
Sulf
Lm
TitanoMag
Or
Bi
Chl
Rt
Zrn
Cal
Ms
250
180
212
150
125
106
90
13.5
11.4
9.6
B
t_1
t_2
Quartz arenite (R018)
Quartz arenite (R020)
Epiclastic rocks
Quartzite
Martell syenite
Granite
Leucogranite
Mafic syenite
Till 096
Till 096 (0.25-0.5mm)
Till 101
Till 101 (0.25-0.5mm)
Till 104
Till 104 (0.25-0.5mm)
Till 112
Till 112 (0.25-0.5mm)
Till 115
Till 115 (0.25-0.5mm)
Till 117
Till 117 (0.25-0.5mm)
Till 124
Till 124 (0.25-0.5mm)
Till 128
Till 128 (0.25-0.5mm)
Till 130
Till 130 (0.25-0.5mm)
Till 135
Till 135 (0.25-0.5mm)

Figure 8

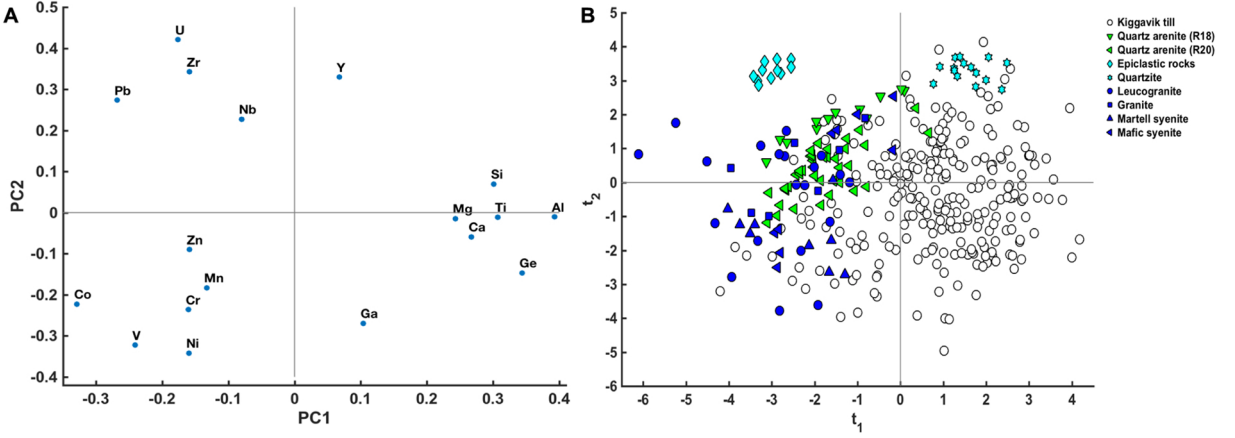
A
U
Zr
Pb
Nb
Y
Si
Mg
Ti
Al
Ca
Zn
Ge
Mn
Co
Cr
Ga
V
Ni
PC2
PC1
B
t_2
t_1
Kiggavik till
Quartz arenite (R18)
Quartz arenite (R20)
Epiclastic rocks
Quartzite
Leucogranite
Granite
Martell syenite
Mafic syenite

Figure 9

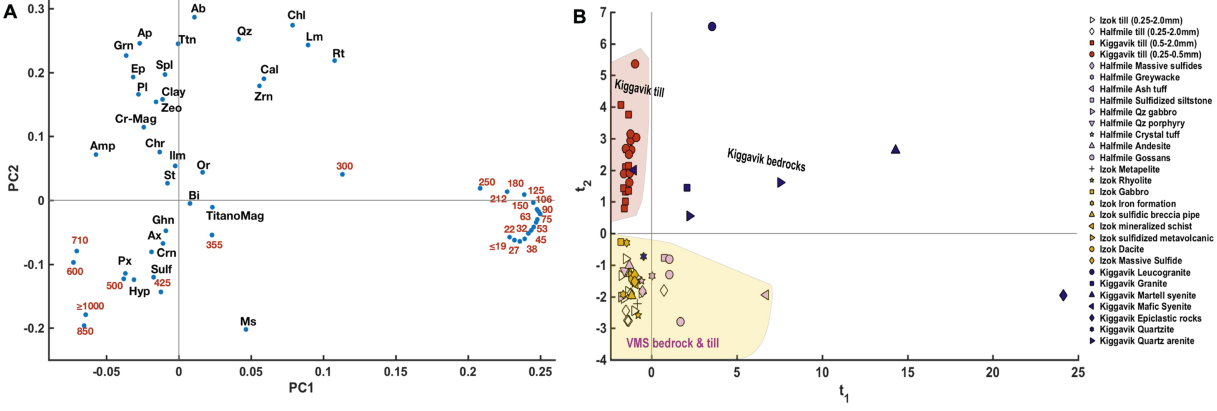
A
PC2
PC1
Ab
Ap
Grn
Ttn
Qz
Chl
Lm
Rt
Ep
Spl
Cal
Pl
Clay
Zrn
Zeo
Cr-Mag
Amp
Chr
Ilm
St
Or
300
Bi
TitanoMag
Ghn
Ax
Crn
355
710
600
Px
Sulf
500
Hyp
425
≥1000
850
Ms
250
180
125
212
150
106
90
63
75
22
32
53
45
≤19
27
38
B
Kiggavik till
Kiggavik bedrocks
VMS bedrock & till
t2
t1
Izok till (0.25-2.0mm)
Halfmile till (0.25-2.0mm)
Kiggavik till (0.5-2.0mm)
Kiggavik till (0.25-0.5mm)
Halfmile Massive sulfides
Halfmile Greywacke
Halfmile Ash tuff
Halfmile Sulfidized siltstone
Halfmile Qz gabbro
Halfmile Qz porphyry
Halfmile Crystal tuff
Halfmile Andesite
Halfmile Gossans
Izok Metapelite
Izok Rhyolite
Izok Gabbro
Izok Iron formation
Izok sulfidic breccia pipe
Izok mineralized schist
Izok sulfidized metavolcanic
Izok Dacite
Izok Massive Sulfide
Kiggavik Leucogranite
Kiggavik Granite
Kiggavik Martell syenite
Kiggavik Mafic Syenite
Kiggavik Epiclastic rocks
Kiggavik Quartzite
Kiggavik Quartz arenite

Figure 10